

Policy Search, Retrieval, and Composition via Task Similarity in Collaborative Agentic Systems

Saptarshi Nath¹, Christos Peridis¹, Eseoghene Benjamin⁴, Xinran Liu², Soheil Kolouri², Peter Kinnell¹, Zexin Li³, Cong Liu³, Shirin Dora¹, Andrea Soltoggio¹

¹Department of Computer Science, Loughborough University, Loughborough, UK

²Department of Electrical Engineering and Computer Science, Vanderbilt University, Nashville, USA

³Department of Electrical Engineering and Computer Engineering, University of California, Riverside, USA

⁴Alan Turing Institute, London, UK

{s.nath, c.peridis, p.kinnell, s.dora, a.soltoggio}@lboro.ac.uk, {xinran.liu, soheil.kolouri}@vanderbilt.edu, {zli536, congli}@ucr.edu, ebenjamin@turing.ac.uk

Abstract

Agentic AI aims to create systems that set their own goals, adapt proactively to change, and refine behavior through continuous experience. Recent advances suggest that, when facing multiple and unforeseen tasks, agents could benefit from sharing machine-learned knowledge and reusing policies that have already been fully or partially learned by other agents. However, how to query, select, and retrieve policies from a pool of agents, and how to integrate such policies remains a largely unexplored area. This study explores how an agent decides what knowledge to select, from whom, and when and how to integrate it in its own policy in order to accelerate its own learning. The proposed algorithm, *Modular Sharing and Composition in Collective Learning* (MOSAIC), improves learning in agentic collectives by combining (1) knowledge selection using performance signals and cosine similarity on Wasserstein task embeddings, (2) modular and transferable neural representations via masks, and (3) policy integration, composition and fine-tuning. MOSAIC outperforms isolated learners and global sharing approaches in both learning speed and overall performance, and in some cases solves tasks that isolated agents cannot. The results also demonstrate that selective, goal-driven reuse leads to less susceptibility to task interference. We also observe the emergence of self-organization, where agents solving simpler tasks accelerate the learning of harder ones through shared knowledge.

Code — <https://github.com/DMIU-ShELL/MOSAIC>

1 Introduction

The ability to solve complex, open-ended problems is an increasingly desirable objective as agentic AI principles become central in AI architectures. In open-ended real-world settings, these systems face challenges in generalizing and adapting to an ever-evolving stream of data and tasks (De Lange et al. 2022; Parisi et al. 2019). Although new lifelong learning algorithms (Kudithipudi et al. 2022) are being introduced to provide continual evolution and adaptation, when agents learn in isolation, they can only benefit from their limited experiences, unlike humans who benefit

from collaboration and sharing of experiences and skills. Recent studies suggest that a shift towards more collaborative types of learning, where agents selectively share and reuse modular knowledge from other agents, is key to reducing redundant learning, accelerating adaptation, and improving robustness (Tarale, Rietman, and Siegelmann 2025; Soltoggio et al. 2024; DARPA/MTO 2021).

In the context of self-adaptation, reinforcement signals provide an effective tool to achieve continuous improvement in a wide range of domains (Sutton and Barto 2018; Jaderberg et al. 2017). In addition, task similarities have been exploited to benefit learning in areas such as transfer learning and multi-task RL (Hendawy, Peters, and D’Eramo 2024; Sun et al. 2022; D’Eramo et al. 2020). Lifelong learning approaches also leverage task similarity when previously learned tasks benefit the learning of subsequent tasks, with an advantage often named *forward transfer* (Ben-Iwhiwhu et al. 2023; Kirkpatrick et al. 2017). However, many approaches to sharing knowledge, e.g., distributed RL (Sartoretti et al. 2019) or Federated Learning (Yoon et al. 2021), often assume some form of centralization and uniformity of tasks, which is ill-suited to the requirements of agentic AI where each agent acts independently, asynchronously, and likely on a large variety of different tasks. Recent studies have begun to investigate the sharing and reuse of policies in evolving multi-agent contexts (Nath et al. 2023; Tarale, Rietman, and Siegelmann 2025; Gerstgrasser, Danino, and Keren 2023). These developments reflect a growing recognition that scalable AI systems increasingly depend on self-directed selective collaboration among autonomous learners.

Knowledge and skill sharing among a set of independent and autonomous learners, while conceptually appealing, presents significant challenges. In particular, open research questions reflect the problems of how to identify what knowledge to acquire, from whom to acquire it, how such knowledge is best represented, and how to integrate it to manifest robust lifelong learning properties (DARPA/MTO 2021; Soltoggio et al. 2024). Furthermore, it is still unclear to what extent collaborative learning offers an advantage over isolated or centralized learning.

To address these questions, this study introduces *Modular Sharing and Composition in Collective Learning* (MO-

SAIC), which describes how agents can select appropriate knowledge from peers with the aim of implementing policy composition and reuse. Problem analysis and the following ablation studies indicate that essential components of such a system are (1) knowledge selection through task similarity, (2) modular and transferable neural representations, and (3) policy integration, composition, and fine-tuning.

Specific algorithmic choices in MOSAIC to implement such components are Wasserstein embeddings for task similarity, transferable binary network masks for sharing, and learnable linear combinations of those to achieve integration and fine tuning. In principle, analogous methods could be used to adapt MOSAIC to a variety of domains, e.g., LoRA-based modular composition for foundation models and LLMs (Hu et al. 2022; He et al. 2022) and embedding methods or descriptors to express task alignment (Achille et al. 2019; Grover et al. 2018; Rakelly et al. 2019).

Simulations indicate that selectively acquiring relevant knowledge is essential to effectively reuse policies. The composition of policies is best achieved with a similarity-driven and reward-aware weighting. The results show how communicating MOSAIC agents learn faster than isolated learners by reusing knowledge from peers on similar tasks. In some cases, communicating agents can solve tasks that they could not learn alone. In addition, the analysis reveals an implicit self-organization, where agents discover and exploit curriculum structures in the available knowledge, resulting in agents building on skills hierarchically, from simpler tasks to learn more complex ones.

In summary, MOSAIC supports the hypothesis that task-relevant policy transfer and reuse, guided by agent-centered optimization objectives, is feasible and effective with advantages over learning in isolation or sharing global parameters, which could lead to task interference. To the best of our knowledge, this is the first study that combines modular and transferable task-specific knowledge with similarity-based selection and integration. Such a combination of components is sufficient to significantly improve sample efficiency and learning through collective knowledge sharing.

2 Related Work

Recent work in modular knowledge reuse for multi-agent RL explores various approaches to enable efficient knowledge transfer. Federated learning methods (Yoon et al. 2021) communicate task-specific masks or binary representations. These approaches lack principled task similarity metrics for selective reuse. MOSAIC addresses this gap through Wasserstein-based similarity measures that guide knowledge selection based on performance signals.

Several frameworks allow parameter-efficient knowledge sharing through masking (Ge et al. 2023; Nath et al. 2023; Gerstgrasser, Danino, and Keren 2023), prototype aggregation (Tan et al. 2022), or decentralized training (Douillard et al. 2024; Jaghoul and Hagemann 2024). Communication-efficient methods reduce information exchange through knowledge preservation and selective sharing (McMahan et al. 2017). These approaches rely on predefined sharing protocols or require synchronous updates. MOSAIC’s binary mask representation enables asyn-

chronous, selective reuse and maintains modularity while minimizing communication overhead.

Policy composition methods like PaCo (Sun et al. 2022) interpolate within shared subspaces. These methods lack mechanisms for similarity-driven integration. Peer-to-peer frameworks (Tarale, Rietman, and Siegelmann 2025; Yu, Vincent, and Schwager 2022) and model-based approaches (Jiang, Narayanan, and Li 2021) enable decentralized coordination. These frameworks do not combine selection with modular representations. MOSAIC combines Wasserstein-based task similarity with binary mask modularity and similarity-driven linear policy combinations. Further discussion of related works is provided in Appendix B.

3 Methodology

The following section describes the components of the MOSAIC algorithm. A high level illustration is provided in Figure 1. Pseudocode can be found in the Appendix F.

3.1 Policy Representations

Isolating task-specific knowledge in compact representations (Alet, Lozano-Perez, and Kaelbling 2018) is a key to making policy transfer easier and more lightweight across agents. Lifelong learning parameter isolation approaches can achieve this goal (Rusu et al. 2016; Mallya and Lazebnik 2018; Wortsman et al. 2020; Ben-Iwhiwhu et al. 2023).

This study adopts neural network masks (Ben-Iwhiwhu et al. 2023; Wortsman et al. 2020) that have shown strong results in lifelong reinforcement learning and supervised learning settings, and supports composition through linear combinations of mask modules. PPO is used for the experiments in this paper; however, the proposed modular composition mechanism is, in principle, agnostic to the choice of RL algorithm. Mask representations rely on a frozen backbone network Φ that is homogeneous across all agents. Each policy π_τ is implicitly parameterized through a sparse mask ϕ_τ , such that $\pi_\tau = \pi_{\Phi \odot g(\phi_\tau)}$, where \odot denotes the Hadamard product, and $g(\cdot)$ is a binarization function applied during the forward pass. The mask ϕ_τ consists of a set of real-valued score vectors, one per layer of the shared backbone network Φ , which select a sparse task-specific subnetwork from Φ without modifying its parameters. Scores are binarized during the forward pass to select a discrete subnetwork from the backbone, given by the thresholding function,

$$g(\phi_\tau)_\ell = \begin{cases} 1 & \text{if } (\phi_\tau)_\ell > \epsilon \\ 0 & \text{otherwise} \end{cases}, \quad \text{with } \epsilon = 0, \quad (1)$$

where $g(\phi_\tau)$ denotes the complete binary mask and ℓ indexes the layers of the backbone network Φ . During the backward pass, gradients are computed with respect to the real-valued mask parameters ϕ_τ , and updates are performed using the straight-through estimator (STE) (Wortsman et al. 2020) to enable learning through the non-differentiable binarization step.

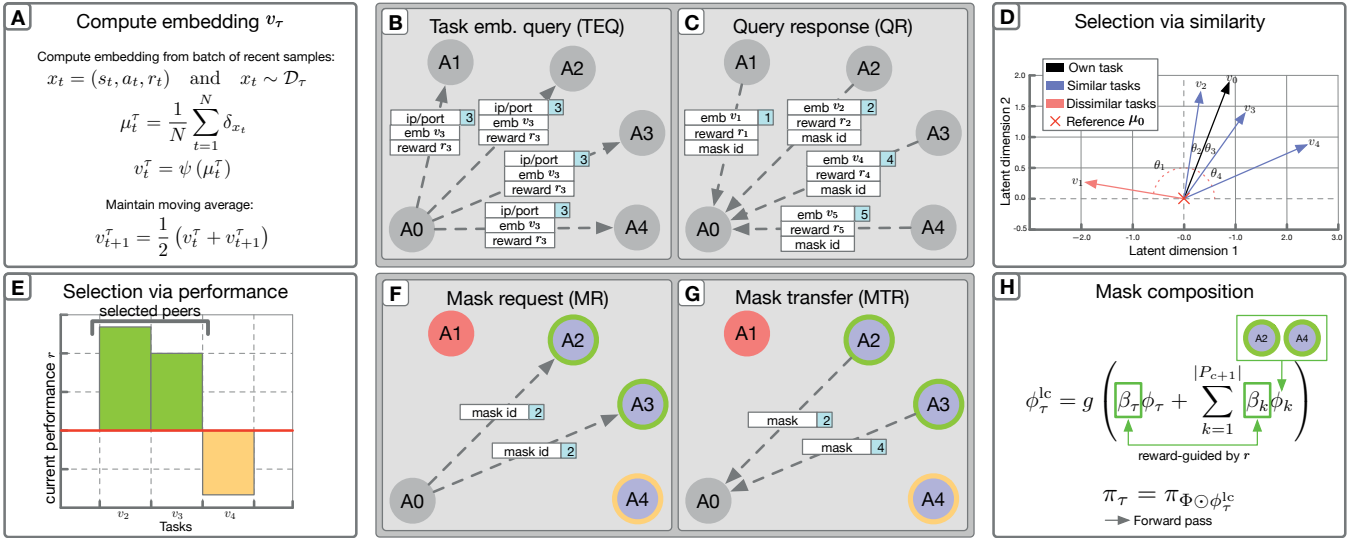


Figure 1: High-level illustration of the main MOSAIC algorithmic steps. (A) A Wasserstein task embedding v_τ is computed from a SAR batch by Agent A0 (representing any agent in the collective). (B) Periodically, the agent A0 broadcasts a task embedding query (TEQ) to all known peers. (C) Peers send back a query response (QR) that contains their task’s v_τ , r , and the corresponding mask ID; (D) Agent A0 selects relevant embeddings using cosine similarity on the Wasserstein embeddings. (E) A0 further selects relevant embeddings using Criterion 1 and Criterion 2. (F) A0 sends mask requests (MR). (G) The contacted agents respond by sending the requested mask through a mask transfer (MTR). (H) Incoming masks from A2 and A3 are incorporated into A0. The training of the agent’s policy occurs in parallel (not represented in the figure).

3.2 Wasserstein Task Embeddings for Online Reinforcement Learning

To identify suitable policies for a given task, MOSAIC extends Liu et al. (2025) to RL by computing embeddings over batches of state-action-reward (SAR) data collected online (see Figure 1(A)). For task τ , the agent maintains an empirical task distribution

$$\mu_\tau = \frac{1}{N} \sum_{t=1}^N \delta_{x_t} \in \mathcal{P}(\mathbb{R}^d), \quad (2)$$

where $x_t = (s_t, a_t, r_t)$ and $x_t \sim \mathcal{D}_\tau$. Here, \mathcal{D}_τ denotes the replay buffer for τ , and each $x_t \in \mathbb{R}^d$ is a state-action-reward (SAR) tuple. The tuple dimensionality is $d = d_s + d_a + d_r$, where d_s, d_a , and d_r are the dimensions of the state, action, and scalar reward, respectively. We use $N = 128$ samples in our experiments. δ_{x_t} denotes the Dirac measure centered on the sample x_t . A fixed synthetic reference distribution μ_0 is defined as

$$\mu_0 = \frac{1}{M} \sum_{m=1}^M \delta_{x_m^0}, \quad (3)$$

where $x_m^0 \sim \text{Uniform}(-1, 1)^d$ is sampled once during initialization and fixed thereafter. We fix $M = 50$ as the number of reference points in the synthetic distribution. This shared reference is used across all agents and enables them to align their embeddings in a shared latent space without centralized training or supervision. The 2-Wasserstein distance between μ_τ and μ_0 is computed by solving the optimal

transport problem,

$$\gamma^* = \arg \min_{\gamma \in \mathbb{R}^{N \times M}} \sum_{t=1}^N \sum_{m=1}^M \gamma_{tm} \|x_t - x_m^0\|^2 \quad (4)$$

s.t. $\gamma_{tm} \geq 0$, $\gamma \mathbf{1}_M = \frac{1}{N} \mathbf{1}_N$, $\gamma^\top \mathbf{1}_N = \frac{1}{M} \mathbf{1}_M$,

where $\mathbf{1}_N$ and $\mathbf{1}_M$ are vectors of ones in \mathbb{R}^N and \mathbb{R}^M , respectively. The Wasserstein task embedding operator ψ maps the task distribution μ_τ to a vector $v_\tau \in \mathbb{R}^{M \times d}$ via the barycenter projection of γ^* on $\{x_t\}_{t=1}^N$,

$$v_\tau = \psi(\mu_\tau) = \left[\sum_{t=1}^N \gamma_{tm}^* x_t \right]_{m=1}^M. \quad (5)$$

This mapping places each task τ in a shared latent space, where metrics can be used to quantify task relationships. A moving average is maintained to smooth fluctuations as the agent’s policy evolves, $v_{t+1}^r = \frac{1}{2} (v_t^r + v_{t+1}^r)$.

3.3 Knowledge Selection and Sharing

Agents communicate by maintaining a list of IP addresses and ports for other agents, which allows them to be located anywhere on the Internet. Each agent $i \in \mathcal{I}$ can communicate directly with all other agents $j \in \mathcal{I}$, $j \neq i$ at any time.

Phase 1: Embedding queries At any time, an agent i can initiate a task embedding query (TEQ) by broadcasting its current task embedding v_i , iteration performance \bar{r}_i , and its IP/port (see Figure 1(B)(C)). Upon receiving the TEQ, each peer agent $j \neq i$ responds with its most recent task embedding v_j and associated performance \bar{r}_j .

Phase 2: Policy selection. Once the agent has received query responses (QR) (see Figure 1(F)(G)) with relevant embeddings from other agents, it computes the cosine similarity between its own embedding and those of each peer,

$$\cos(v_i, v_j) = \frac{\langle \text{vec}(v_i), \text{vec}(v_j) \rangle}{|\text{vec}(v_i)| \cdot |\text{vec}(v_j)|}, \quad \cos \in [-1, 1]. \quad (6)$$

To identify useful policies, agent i applies two heuristic filters based on similarity and performance:

$$\mathbb{I}_{\text{align}}(i, j) = \begin{cases} 1 & \text{if } \cos(v_i, v_j) > \theta, \\ 0 & \text{otherwise} \end{cases} \quad (\text{Criterion 1})$$

$$\mathbb{I}_{\text{perf}}(i, j) = \begin{cases} 1 & \text{if } \bar{r}_j > \bar{r}_i, \\ 0 & \text{otherwise} \end{cases} \quad (\text{Criterion 2})$$

with $\theta = 0.5$ in all experiments. The first criterion promotes semantic alignment between tasks, revealing latent similarities that can lead to effective transfer (see Section 4.4). The second ensures that agents only acquire masks from peers whose performance exceeds their own, avoiding noisy or under-trained policies that can degrade performance. Criterion 2 guards against the frequent false positives seen when comparing poorly trained policies that yield deceptively similar embeddings.

The two phases and the selection criteria also result in a bandwidth-efficient approach, since policies are transferred only when considered potentially useful. The peer masks that pass both criteria are stored as the set $P_{c+1} = \{\phi_1, \dots, \phi_K\}$, where each ϕ_k denotes a mask received from a selected peer.

3.4 Knowledge Composition and Fine Tuning

Masks received from other agents meeting the two selection criteria above have been pretrained on tasks that are likely related to or share similarities with the agent’s current task. As previously shown in Ben-Iwhiwhu et al. (2023), a linear combination of masks, weighted with trainable parameters β , can lead to beneficial policy search in RL. MOSAIC exploits this idea by combining policies that have been trained on the local agent, plus those acquired from other agents. In this study, the β values are computed using softmax on a set of beta parameters, optimized in log-space, $\tilde{\beta} \in \mathbb{R}^{1+|P_c|}$, where P_c is the number of masks acquired during a communication event c . During the forward pass, the agent constructs the linearly combined, binarized mask,

$$\phi_\tau^{\text{lc}} = g \left(\beta_\tau \phi_\tau + \sum_{k=1}^{|P_{c+1}|} \beta_k \phi_k \right), \quad (7)$$

where ϕ_τ is the agent’s own task mask, and ϕ_k is the k -th peer mask. The parameters β_τ and β_k are the softmax-normalized values derived from $\tilde{\beta}$, for ϕ_τ and ϕ_k , respectively. $|P_{c+1}|$ is the number of masks acquired in the next communication event. The resulting binary mask, ϕ_τ^{lc} , is then used to modulate the backbone parameters, which gives the final policy π_τ . As training continues on the local task, the agent updates the β parameters and the real value ϕ_τ via backpropagation (keeping all ϕ_k masks fixed) thus fine tuning the overall resulting policy determined by ϕ_τ^{lc} .

Reward-Guided Initialization (RGI). The trainable parameters, β , enable gradient descent to determine which policies are most useful for the current task. The initial weighting as the masks are received is given by,

$$\beta_\tau = 0.5 + 0.5\bar{r}, \quad \beta_k = \frac{0.5(1 - \bar{r})}{|P_{c+1}|}, \quad (8)$$

where $\bar{r} \in [0, 1]$ is the agent’s normalized return from the last iteration. This scheme biases low-performing agents toward external knowledge and high-performing agents toward their own policies. Ablation studies show that such an initialization provides a strong advantage, even though β is later tuned by gradient descent.

Before integrating a new set of peer masks P_{c+1} , the agent consolidates its current task mask ϕ_τ with the previous peer masks P_c using a weighted linear combination,

$$\phi_\tau \leftarrow \beta_\tau \phi_\tau + \sum_{k=1}^{|P_c|} \beta_k \phi_k. \quad (9)$$

The consolidation collapses multiple masks into one without affecting the policy, managing memory scalability.

4 Experiments

MOSAIC is evaluated on three sparse-reward reinforcement learning benchmarks. The CT-graph (Soltoggio et al. 2023) and MiniHack MultiRoom (Samvelyan et al. 2021) are used to assess the advantage of communicating agents versus isolated agents. The MiniGrid Crossing (Chevalier-Boisvert, Willems, and Pal 2018) is used to assess the performance of MOSAIC against the chosen baselines. Each benchmark includes tasks with similar, dissimilar, and interfering tasks to assess whether MOSAIC can identify and leverage the available task similarities, while avoiding interfering policies. Each agent is assigned a unique task and trained in parallel with other agents. PPO (Schulman et al. 2017) was used in all experiments, with an FCN for MiniGrid and CT-graph, and a CNN for MiniHack. Individual results are shown in Appendix E, Figures 14, 15, and 16. Details on computing infrastructure, hyperparameters, architectures, and libraries are reported in the Appendix F, Tables 5, 6, 8, and 7. Appendix A, Table 3 reports significance testing.

4.1 Image Sequence Learning

The image sequence learning (ISL) benchmark, implemented with the Configurable Tree Graph (CT-Graph) environment (Soltoggio et al. 2023), consists of procedurally generated tree navigation problems where each node is an RL state encoded as an image. We define a curriculum of 28 tasks organized into four independent image sets, each containing seven related tasks of increasing tree depth (2–8). This configuration produces four distinct and unrelated task groups with internal hierarchies of difficulty, from easy (depth 2) to very hard (depth 8). Sparse rewards and exponential branching make the benchmark challenging, with reward probabilities as low as $\approx 7.74 \times 10^{-9}$ for depth-8 tasks (Soltoggio et al. 2023).

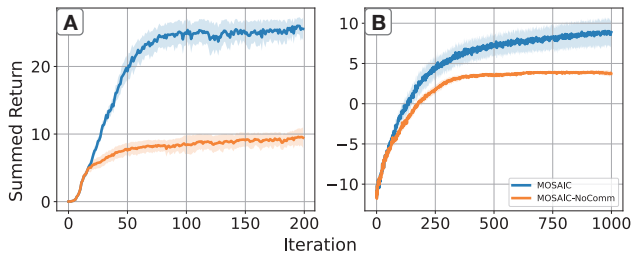


Figure 2: Performance of communicating MOSAIC agents versus isolated agents on the same tasks. (A) Image sequence learning, 28 tasks, five seeds/task: average of 140 runs with 95% confidence intervals (Colas, Sigaud, and Oudeyer 2018). (B) MiniHack Multiroom, 14 tasks, five seeds/task: average of 70 runs with 95% confidence intervals. MOSAIC agents achieve relative gains of 170.8% and 128.2% over the isolated baseline in the image sequence and MiniHack benchmarks, respectively.

Results in Figure 2(A) show that MOSAIC achieves significantly faster learning and broader task coverage, outperforming MOSAIC-NoComm (no sharing among agents) by 2.7 \times , reaching a maximum total return of 26.0 across all 28 tasks. MOSAIC reaches 50% performance (total return of 14) in 37 iterations (18,944 steps). MOSAIC-NoComm plateaus at a maximum of 9.6. On average, MOSAIC-NoComm fails on 18 tasks, whereas MOSAIC fails on only 2.

4.2 MiniHack MultiRoom

MiniHack is a grid-based navigation task with sparse rewards and pixel observations. Agents must traverse connected rooms to reach a final goal. We evaluate MOSAIC on 14 tasks grouped into two difficulty clusters: room sizes of 4×4 and 6×6 . Each level adds a room connected by a closed but unlocked door. Agents receive +1 for task completion and -0.01 for collisions. Task layouts are randomized every episode to enable learning of behavioral strategies as opposed to trajectories. As shown in Figure 2(B), MOSAIC agents reach zero reward by iteration 132 (270,336 steps) versus iteration 176 (360,448 steps) for MOSAIC-NoComm, which is a 25% reduction in the required samples. Over the full run, MOSAIC attains a maximum total return of 9.04 across all tasks, compared to 3.96 for MOSAIC-NoComm.

4.3 MiniGrid Crossing

The MiniGrid benchmark is a sparse-reward grid-world navigation task with symbolic observations. MOSAIC is evaluated on 14 tasks spanning seven SimpleCrossing and seven LavaCrossing variants, which differ in layout, object placement, and room structure. Total return curves for all methods are shown in Figure 3, with final and intermediate metrics in Table 1. MOSAIC is compared against the following baselines: Multi-Task PPO (MTPPO) uses a shared backbone without modularity or interference mitigation. Multi-DQN (MDQN) (D’Eramo et al. 2020) attaches task-specific Q-

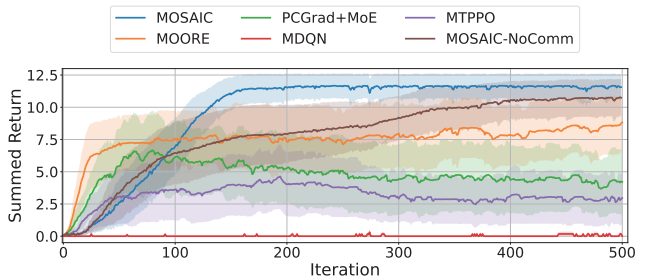


Figure 3: Comparison of MOSAIC to baseline approaches on the 14 task MiniGrid curricula made up of SimpleCrossing and LavaCrossing task variations: average performance for 70 runs with 95% confidence intervals.

Method	Final perf	25% perf	50% perf	75% perf
MOSAIC (ours)	11.67	55	90	119
MTPPO	4.64	48	-	-
MDQN	0.31	-	-	-
PCGrad+MoE	6.66	24	54	-
MOORE	8.83	13	24	-
MOSAIC-NoComm	10.78	46	87	291

Table 1: Performance metrics on the MiniGrid Crossing benchmark. The table reports the final average return and the number of iterations to reach 25%, 50% and 75% of the theoretical maximum. Dashes indicate that the thresholds were not reached during the training.

heads to a shared encoder but has no mechanism to avoid interference. PCGrad+MoE (Yu et al. 2020) combines a shared encoder, expert subnetworks, and gradient projection to resolve conflicts. Mixture of Orthogonal Experts (MOORE) (Hendawy, Peters, and D’Eramo 2024) promotes expert diversity via orthogonalization with learned gating to reduce overlap. MOSAIC achieves the highest final return (11.67), outperforming all baselines. MTPPO peaks at 4.64 (30% of the theoretical maximum), while MDQN fails to learn any tasks, peaking at 0.31. MOORE and PCGrad+MoE improve faster early, reaching 50% thresholds in 24 (49,152 steps) and 54 iterations (110,592 steps) respectively, but plateau well below MOSAIC and never exceed 75%. We speculate that centralized models with gradient sharing (MTPPO, PCGrad+MoE) achieve early gains through shared features but suffer interference that limits long-term specialization.

4.4 How Similarity Helps Targeted Policy Transfers

Figure 4 illustrates the average cosine similarity in the CT-graph benchmark between task embeddings and the converged consolidation parameters $\hat{\beta}_j^i$ (see Eq. (9)), which provides an indication of the influence of policies derived from task j when learning task i .

The cosine similarities of tasks presented in random order (Figure 4(A)), when clustered with WPGMA (Figure 4(C)), allow for the reconstruction of the four groups of tasks, and

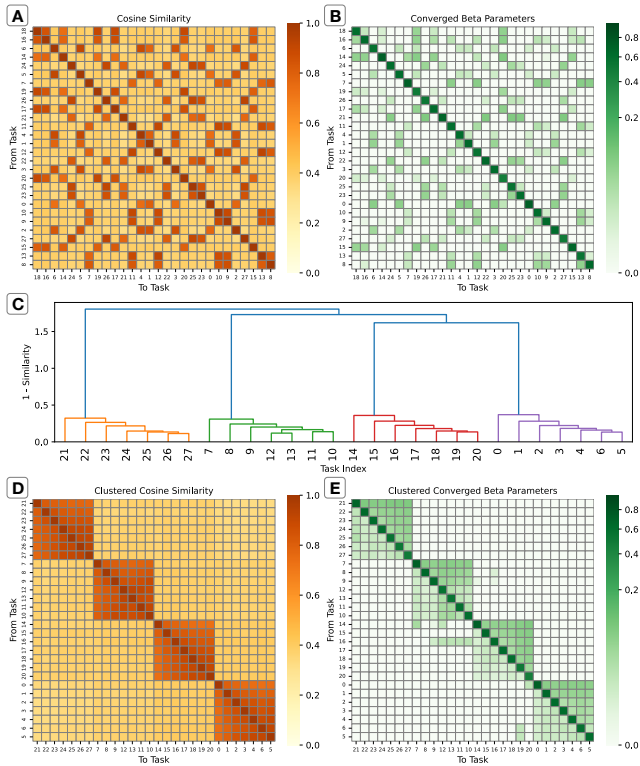


Figure 4: Pairwise cosine similarity and $\hat{\beta}$ statistics in the image sequence learning benchmark. (A) Cosine similarity matrix. (B) $\hat{\beta}$ values indicating policy use per task. (C) Cosine similarities clustered using WPGMA, shown as a dendrogram. (D) Cosine similarity matrix reordered by clustering. (E) Clustered $\hat{\beta}$ values show that similar tasks exhibit the highest policy reuse. Annotated heatmaps of individual clusters are in Appendix E.1, Figure 17.

even the inter-group difficulty relationship. By reordering the matrix using a such clustering, Figure 4(D) illustrates visually the successful reconstruction of task relationships. The $\hat{\beta}$ matrices (Figures 4(B) and (E)) confirm that policy reuse and task similarity remain similar even after fine tuning of the policies. Note that, unlike the symmetric similarity matrix, $\hat{\beta}$ values are asymmetric, reflecting source-to-target policy reuse.

Figure 5 presents the performance of agents in the CT-graph grouped by difficulty levels. Interestingly, comparing with isolated learning (bottom graph) suggests that the policies of easier tasks are progressively shared with agents solving harder tasks. This coordination enabling those agents to find successful policies that the same RL algorithm fails to discover when learning in isolation. This analysis helps explain the 170.8% performance gain of communicating agents over isolated agents (Figure 2(A)): agents tackling harder tasks retrieve, combine, and refine policies from simpler tasks to solve complex problems.

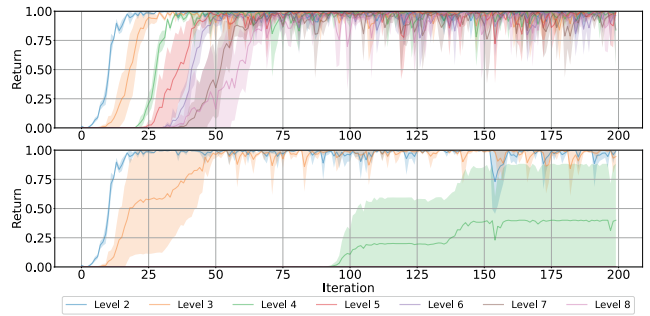


Figure 5: Performance grouped by task complexity, i.e., seven different levels, corresponding to different graph depths, in the image sequence learning problem. Average performance for 20 runs (four tasks and five seeds/task) with 95% confidence intervals. Communicating MOSAIC agents (top graph) are compared with isolated MOSAIC agents (bottom graph). Communicating agents solve tasks progressively, from the simplest to the hardest tasks. Isolated agents only manage to solve the two simplest tasks, and partially the third, but fail on the four most complex tasks.

4.5 Ablation Studies

Ablation studies were conducted to assess the effect on performance of MOSAIC’s knowledge selection criteria and reward-guided initialization (RGI) on performance. Figure 6 compares three ablated variants of MOSAIC: without cosine similarity-based selection (\neg Criterion 1), without performance-based selection (\neg Criterion 2), and without reward-guided weight initialization (\neg RGI). MOSAIC-NoComm is included as a reference baseline.

\neg Criterion 1 reaches a total return of 20.1, whereas MOSAIC reaches 26.0, outperforming it by a factor of 1.29. We speculate that this gap could widen further in settings in which the number of unrelated tasks grows, i.e., where selecting the most relevant knowledge becomes critical.

\neg Criterion 2 performs comparable to MOSAIC at the end of training (25.6), but exhibits significantly slower learning. This behavior makes sense because as agents improve their performance, prioritizing higher reward becomes less critical. These two ablations \neg Criterion 1 and \neg Criterion 2 reach 50% of the theoretical maximum (14.0) in 76 (38,912 steps) and 71 iterations (36,352 steps), respectively. MOSAIC reaches this threshold in 37 iterations (18,944 steps), reaching 50% performance 1.9 \times and 2.0 \times faster, respectively.

\neg RGI removes reward-guided initialization and instead uses a fixed weighting of 0.5 for the local policy and 0.5 for external policies. This experiment performs comparably with MOSAIC; however, the average return shows periodic instability, characterized by sharp performance drops coinciding with communication events, resembling a sawtooth pattern. This behavior suggests that RGI is crucial to learning stability when integrating external masks.

Further ablation studies are shown in Appendix D to test the impact of query frequency on the performance of MOSAIC, and the impacts of the number of samples and size of

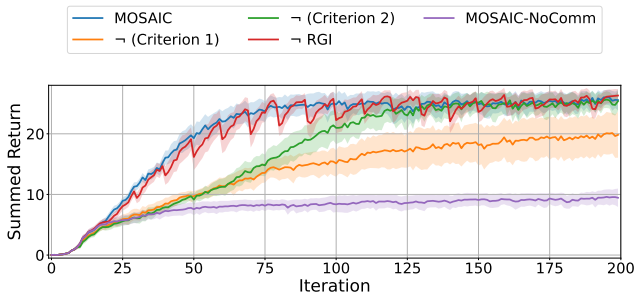


Figure 6: Ablation studies showing average performance over 140 runs (28 tasks, five seeds per task), with 95% confidence intervals. Variants tested include MOSAIC with no similarity criterion (\neg Criterion 1), no reward criterion (\neg Criterion 2), or no reward-guided initialization (\neg RGI). MOSAIC-NoComm is included as a baseline. Removing any of these components significantly degrades performance, highlighting their combined importance.

the reference distribution on embedding accuracy and performance.

5 Discussion

The results show that MOSAIC’s principles are effective across diverse settings. Agents achieved faster and more successful learning dynamics than isolated agents. In particular, transferring masks from some tasks accelerated learning in other tasks, consistent with findings in centralized lifelong learning (Ben-Iwhiwhu et al. 2023). These gains were most evident in reward-sparse and hierarchical environments, where agents that learned simpler tasks supported those that learned harder ones (Florensa et al. 2018; Nachum et al. 2018).

The ablation study highlights the importance of selection based on relevance and utility and of reward-adjusted weighting when integrating new policies. Naïve sharing overwrites stable learning (Isele and Cosgun 2018), deteriorating performance. These results emphasize the importance of selection when the available tasks and curriculum are unknown (Foerster et al. 2016). The effect of reward-guided initialization suggests that careful policy weighting is important to avoid performance disruption before fine tuning.

It is worth noting that MOSAIC’s design takes inspiration from lifelong learning algorithms. Thus, policy composition can easily be extended to previously learned policies of past tasks. Such an extension could deal with continuous streams of evolving tasks (Serra et al. 2018), supporting scalable and open-ended lifelong learning.

Limitations. Although the experiments were conducted in simulation, MOSAIC is designed for decentralized, bandwidth-limited deployments (e.g., robot fleets, on-device perception). Agents exchange only compact embeddings and mask scores while inference stays on-device. Key deployment considerations are cross-site normalization, private/authenticated exchange, and tuning query frequency and size to fit bandwidth.

MOSAIC relies on raw per-iteration reward as a selection and weighting signal, which limits generalization to environments with differing reward functions. Reward-normalized scores or task-progress metrics could improve environment-agnostic reuse. Adaptive or sparse topologies would better mitigate bandwidth scalability constraints (Tang et al. 2024). The policy composition used in MOSAIC is limited to positive combinations only. Other composition or mixture approaches could be tested (He et al. 2022). Alternative modular skill representations could be used for applications to larger neural networks, e.g., LoRA-like modules and adapters for transformer architectures (Hu et al. 2022; He et al. 2022). In all such cases, the requirement for a shared backbone or foundation model can reduce the pool of agents able to share knowledge and limit long-term development of progressively more complex skills (Houlsby et al. 2019).

Communication and selection mechanisms in MOSAIC were introduced as a proof-of-concept to test whether selective transfer is essential for agentic knowledge reuse (DARPA/MTO 2021; Soltoggio et al. 2024). Allowing policies to learn when and how to communicate could further increase autonomy (Foerster et al. 2016), but dynamic communication policies raise safety concerns. Agents could learn uncooperative strategies, exploit collective knowledge without contributing, or share harmful policies. Such risks mirror classic game-theoretic challenges and require safeguards. MOSAIC-like systems may also face adversarial attacks exploiting the agent-to-agent nature through model poisoning or policy extraction.

6 Conclusion

This work introduced Modular Sharing and Composition in Collective Learning (MOSAIC), where agents search, retrieve, and compose policies obtained from peers learning other tasks. The collective was shown to significantly outperform isolated agents by selecting and fine-tuning task-aligned knowledge. Results show that policy sharing is most effective when implemented selectively, with policy weighting and fine-tuning. Selection also results in the discovery of implicit curricula where simpler tasks help agents learn complex ones faster.

MOSAIC improves interpretability, as composed policies are traceable to their sources and the approach could extend to domains such as language, perception, and control. However, autonomous knowledge sharing carries risks: flawed or misaligned policies may spread rapidly. Future work must ensure that transfers remain safe and aligned with agent objectives. Using selective and modular reuse, MOSAIC can support scalable, adaptive, and collaborative agentic AI in real-world applications.

Acknowledgements

This material is based upon work supported by the Defense Advanced Research Projects Agency (DARPA) under contract No. HR001121901 (Shared Experience Lifelong Learning) and the Industrial Robots-as-a-Service (IRaaS) project funded by the EPSRC (EP/V050966/1).

References

- Achille, A.; Lam, M.; Tewari, R.; Ravichandran, A.; Maji, S.; Fowlkes, C. C.; Soatto, S.; and Perona, P. 2019. Task2Vec: Task Embedding for Meta-Learning. In *Proceedings of the IEEE/CVF International Conference on Computer Vision (ICCV)*.
- Alet, F.; Lozano-Perez, T.; and Kaelbling, L. P. 2018. Modular Meta-Learning. In Billard, A.; Dragan, A.; Peters, J.; and Morimoto, J., eds., *Proceedings of The 2nd Conference on Robot Learning*, volume 87 of *Proceedings of Machine Learning Research*, 856–868. PMLR.
- Andreas, J.; Rohrbach, M.; Darrell, T.; and Klein, D. 2016. Neural Module Networks. In *2016 IEEE Conference on Computer Vision and Pattern Recognition (CVPR)*, 39–48.
- Araki, B.; Li, X.; Vodrahalli, K.; Decastro, J.; Fry, M.; and Rus, D. 2021. The Logical Options Framework. In Meila, M.; and Zhang, T., eds., *Proceedings of the 38th International Conference on Machine Learning*, volume 139 of *Proceedings of Machine Learning Research*, 307–317. PMLR.
- Ben-Iwhiwhu, E.; Nath, S.; Pilly, P. K.; Kolouri, S.; and Soltoggio, A. 2023. Lifelong Reinforcement Learning with Modulating Masks. *Transactions on Machine Learning Research*.
- Chevalier-Boisvert, M.; Willems, L.; and Pal, S. 2018. Minimalistic Gridworld Environment for OpenAI Gym. <https://github.com/maximecb/gym-minigrid>.
- Chu, W.-S.; De La Torre, F.; and Cohn, J. F. 2013. Selective Transfer Machine for Personalized Facial Action Unit Detection. In *Proceedings of the IEEE Conference on Computer Vision and Pattern Recognition (CVPR)*.
- Chu, Z.; Cai, R.; and Wang, H. 2024. Meta-Reinforcement Learning via Exploratory Task Clustering. In *Proceedings of the Thirty-Eighth AAAI Conference on Artificial Intelligence and Thirty-Sixth Conference on Innovative Applications of Artificial Intelligence and Fourteenth Symposium on Educational Advances in Artificial Intelligence, AAAI'24/IAAI'24/EAAI'24*. AAAI Press. ISBN 978-1-57735-887-9.
- Colas, C.; Sigaud, O.; and Oudeyer, P.-Y. 2018. How Many Random Seeds? Statistical Power Analysis in Deep Reinforcement Learning Experiments. *arXiv preprint arXiv:1806.08295*.
- DARPA/MTO. 2021. Artificial Intelligence Exploration (AIE) Opportunity DARPA-PA-20-02-11 Shared-Experience Lifelong Learning (ShELL). <https://sam.gov/opp/1afbf600f2e04b26941fad352c08d1f1/view>. Accessed 2023/10/10.
- De Lange, M.; Aljundi, R.; Masana, M.; Parisot, S.; Jia, X.; Leonardis, A.; Slabaugh, G.; and Tuytelaars, T. 2022. A Continual Learning Survey: Defying Forgetting in Classification Tasks. *IEEE Transactions on Pattern Analysis and Machine Intelligence*, 44(7): 3366–3385.
- D’Eramo, C.; Tateo, D.; Bonarini, A.; Restelli, M.; and Peters, J. 2020. Sharing Knowledge in Multi-Task Deep Reinforcement Learning. In *International Conference on Learning Representations*.
- Devvrit; Kudugunta, S.; Kusupati, A.; Dettmers, T.; Chen, K.; Dhillon, I.; Tsvetkov, Y.; Hajishirzi, H.; Kakade, S.; Farhadi, A.; and Jain, P. 2024. MatFormer: Nested Transformer for Elastic Inference. *arXiv:2310.07707*.
- Dick, J.; Ladosz, P.; Ben-Iwhiwhu, E.; Shimadzu, H.; Kinnell, P.; Pilly, P. K.; Kolouri, S.; and Soltoggio, A. 2020. Detecting changes and avoiding catastrophic forgetting in dynamic partially observable environments. *Frontiers in neurobotics*, 14: 578675.
- Dick, J.; Nath, S.; Peridis, C.; Benjamin, E.; Kolouri, S.; and Soltoggio, A. 2024. Statistical Context Detection for Deep Lifelong Reinforcement Learning. *arXiv:2405.19047*.
- Dognin, P.; Melnyk, I.; Mroueh, Y.; Ross, J.; Santos, C. D.; and Sercu, T. 2019. Wasserstein Barycenter Model Ensembling. *arXiv:1902.04999*.
- Douillard, A.; Feng, Q.; Rusu, A. A.; Kuncoro, A.; Donchev, Y.; Chhaparia, R.; Gog, I.; Ranzato, M.; Shen, J.; and Szlam, A. 2024. DiPaCo: Distributed Path Composition. *arXiv:2403.10616*.
- Fedus, W.; Zoph, B.; and Shazeer, N. 2022. Switch Transformers: Scaling to Trillion Parameter Models with Simple and Efficient Sparsity. *J. Mach. Learn. Res.*, 23(1).
- Finn, C.; Abbeel, P.; and Levine, S. 2017. Model-Agnostic Meta-Learning for Fast Adaptation of Deep Networks. In *International conference on machine learning*, 1126–1135. PMLR.
- Florensa, C.; Held, D.; Geng, X.; and Abbeel, P. 2018. Automatic Goal Generation for Reinforcement Learning Agents. In Dy, J.; and Krause, A., eds., *Proceedings of the 35th International Conference on Machine Learning*, volume 80 of *Proceedings of Machine Learning Research*, 1515–1528. PMLR.
- Foerster, J. N.; Assael, Y. M.; de Freitas, N.; and Whiteson, S. 2016. Learning to Communicate with Deep Multi-Agent Reinforcement Learning. In *Proceedings of the 30th International Conference on Neural Information Processing Systems, NIPS’16*, 2145–2153. Red Hook, NY, USA: Curran Associates Inc. ISBN 9781510838819.
- Frogner, C.; Mirzazadeh, F.; and Solomon, J. 2019. Learning Embeddings into Entropic Wasserstein Spaces. *arXiv:1905.03329*.
- Ge, Y.; Li, Y.; Wu, D.; Xu, A.; Jones, A. M.; Rios, A. S.; Fostiropoulos, I.; Huang, P.-H.; Murdock, Z. W.; Sahin, G.; et al. 2023. Lightweight Learner for Shared Knowledge Lifelong Learning. *Transactions on Machine Learning Research*.
- Gerstgrasser, M.; Danino, T.; and Keren, S. 2023. Selectively Sharing Experiences Improves Multi-Agent Reinforcement Learning. In *Thirty-seventh Conference on Neural Information Processing Systems*.
- Grover, A.; Al-Shedivat, M.; Gupta, J.; Burda, Y.; and Edwards, H. 2018. Learning Policy Representations in Multi-agent Systems. In Dy, J.; and Krause, A., eds., *Proceedings of the 35th International Conference on Machine Learning*, volume 80 of *Proceedings of Machine Learning Research*, 1802–1811. PMLR.

- Gummadi, M.; Kent, D.; Mendez, J. A.; and Eaton, E. 2022. SHELS: Exclusive Feature Sets for Novelty Detection and Continual Learning Without Class Boundaries. In Chandar, S.; Pascanu, R.; and Precup, D., eds., *Proceedings of The 1st Conference on Lifelong Learning Agents*, volume 199 of *Proceedings of Machine Learning Research*, 1065–1085. PMLR.
- Guo, Y.; Shi, H.; Kumar, A.; Grauman, K.; Rosing, T.; and Feris, R. 2018. SpotTune: Transfer Learning through Adaptive Fine-tuning. arXiv:1811.08737.
- Gururangan, S.; Marasović, A.; Swayamdipta, S.; Lo, K.; Beltagy, I.; Downey, D.; and Smith, N. A. 2020. Don't Stop Pretraining: Adapt Language Models to Domains and Tasks. In Jurafsky, D.; Chai, J.; Schluter, N.; and Tetreault, J., eds., *Proceedings of the 58th Annual Meeting of the Association for Computational Linguistics*, 8342–8360. Online: Association for Computational Linguistics.
- He, J.; Zhou, C.; Ma, X.; Berg-Kirkpatrick, T.; and Neubig, G. 2022. Towards a Unified View of Parameter-Efficient Transfer Learning. In *International Conference on Learning Representations*.
- Hendawy, A.; Peters, J.; and D'Eramo, C. 2024. Multi-Task Reinforcement Learning with Mixture of Orthogonal Experts. In *The Twelfth International Conference on Learning Representations*.
- Henderson, P.; Islam, R.; Bachman, P.; Pineau, J.; Precup, D.; and Meger, D. 2018. Deep Reinforcement Learning That Matters. *Proceedings of the AAAI Conference on Artificial Intelligence*, 32(1).
- Houlsby, N.; Giurgiu, A.; Jastrzebski, S.; Morrone, B.; De Laroussilhe, Q.; Gesmundo, A.; Attariyan, M.; and Gelly, S. 2019. Parameter-Efficient Transfer Learning for NLP. In Chaudhuri, K.; and Salakhutdinov, R., eds., *Proceedings of the 36th International Conference on Machine Learning*, volume 97 of *Proceedings of Machine Learning Research*, 2790–2799. PMLR.
- Hu, E. J.; yelong shen; Wallis, P.; Allen-Zhu, Z.; Li, Y.; Wang, S.; Wang, L.; and Chen, W. 2022. LoRA: Low-Rank Adaptation of Large Language Models. In *International Conference on Learning Representations*.
- Huang, H.; Ye, D.; Shen, L.; and Liu, W. 2023. Curriculum-Based Asymmetric Multi-Task Reinforcement Learning. *IEEE Transactions on Pattern Analysis and Machine Intelligence*, 45(6): 7258–7269.
- Isele, D.; and Cosgun, A. 2018. Selective Experience Replay for Lifelong Learning. *Proceedings of the AAAI Conference on Artificial Intelligence*, 32(1).
- Jaderberg, M.; Mnih, V.; Czarnecki, W. M.; Schaul, T.; Leibo, J. Z.; Silver, D.; and Kavukcuoglu, K. 2017. Reinforcement Learning with Unsupervised Auxiliary Tasks. In *International Conference on Learning Representations*.
- Jaghoul, S.; and Hagemann, J. 2024. OpenDiLoCo: An Open-Source Framework for Globally Distributed Low-Communication Training. In *Workshop on Efficient Systems for Foundation Models II @ ICML2024*.
- Jang, Y.; Lee, H.; Hwang, S. J.; and Shin, J. 2019. Learning What and Where to Transfer. arXiv:1905.05901.
- Jiang, W. C.; Narayanan, V.; and Li, J. S. 2021. Model Learning and Knowledge Sharing for Cooperative Multi-agent Systems in Stochastic Environment. *IEEE Transactions on Cybernetics*, 51(12): 5717–5727.
- Kirkpatrick, J.; Pascanu, R.; Rabinowitz, N.; Veness, J.; Desjardins, G.; Rusu, A. A.; Milan, K.; Quan, J.; Ramalho, T.; Grabska-Barwinska, A.; et al. 2017. Overcoming catastrophic forgetting in neural networks. *Proceedings of the national academy of sciences*, 114(13): 3521–3526.
- Kolouri, S.; Naderializadeh, N.; Rohde, G. K.; and Hoffmann, H. 2021. Wasserstein Embedding for Graph Learning. In *International Conference on Learning Representations*.
- Komatsuzaki, A.; Puigcerver, J.; Lee-Thorp, J.; Ruiz, C. R.; Mustafa, B.; Ainslie, J.; Tay, Y.; Dehghani, M.; and Houlsby, N. 2023. Sparse Upcycling: Training Mixture-of-Experts from Dense Checkpoints. arXiv:2212.05055.
- Koster, N.; Grothe, O.; and Rettinger, A. 2022. Signing the Supermask: Keep, Hide, Invert. In *International Conference on Learning Representations*.
- Kudithipudi, D.; Aguilar-Simon, M.; Babb, J.; Bazhenov, M.; Blackiston, D.; Bongard, J.; Brna, A. P.; Chakravarthi Raja, S.; Cheney, N.; Clune, J.; Daram, A.; Fusi, S.; Helfer, P.; Kay, L.; Ketz, N.; Kira, Z.; Kolouri, S.; Krichmar, J. L.; Kriegman, S.; Levin, M.; Madireddy, S.; Manicka, S.; Marjaninejad, A.; McNaughton, B.; Miikkulainen, R.; Navratilova, Z.; Pandit, T.; Parker, A.; Pilly, P. K.; Risi, S.; Sejnowski, T. J.; Soltoggio, A.; Soures, N.; Tolia, A. S.; Urbina-Meléndez, D.; Valero-Cuevas, F. J.; Van de Ven, G. M.; Vogelstein, J. T.; Wang, F.; Weiss, R.; Yanguas-Gil, A.; Zou, X.; and Siegelmann, H. 2022. Biological underpinnings for lifelong learning machines. *Nature Machine Intelligence*, 4(3): 196–210.
- Laskin, M.; Srinivas, A.; and Abbeel, P. 2020. CURL: Contrastive Unsupervised Representations for Reinforcement Learning. In III, H. D.; and Singh, A., eds., *Proceedings of the 37th International Conference on Machine Learning*, volume 119 of *Proceedings of Machine Learning Research*, 5639–5650. PMLR.
- Levy, A.; Konidaris, G.; Platt, R.; and Saenko, K. 2019. Learning Multi-Level Hierarchies with Hindsight. arXiv:1712.00948.
- Li, M.; Piccoli, E.; Lomonaco, V.; and Bacciu, D. 2024. I Know How: Combining Prior Policies to Solve New Tasks. In *2024 IEEE Conference on Games (CoG)*, 1–4.
- Liu, X.; Bai, Y.; Lu, Y.; Soltoggio, A.; and Kolouri, S. 2025. Wasserstein Task Embedding for Measuring Task Similarities. *Neural Networks*, 181: 106796.
- Mallya, A.; Davis, D.; and Lazebnik, S. 2018. Piggyback: Adapting a Single Network to Multiple Tasks by Learning to Mask Weights. In *Proceedings of the European Conference on Computer Vision (ECCV)*, 67–82.
- Mallya, A.; and Lazebnik, S. 2018. Packnet: Adding Multiple Tasks to a Single Network by Iterative Pruning. In *Proceedings of the IEEE conference on Computer Vision and Pattern Recognition*, 7765–7773.

- McMahan, B.; Moore, E.; Ramage, D.; Hampson, S.; and Arcas, B. A. y. 2017. Communication-Efficient Learning of Deep Networks from Decentralized Data. In Singh, A.; and Zhu, J., eds., *Proceedings of the 20th International Conference on Artificial Intelligence and Statistics*, volume 54 of *Proceedings of Machine Learning Research*, 1273–1282. PMLR.
- Mendez, J. A.; and Eaton, E. 2021. Lifelong Learning of Compositional Structures. In *International Conference on Learning Representations*.
- Mendez, J. A.; van Seijen, H.; and Eaton, E. 2022. Modular Lifelong Reinforcement Learning via Neural Composition. In *International Conference on Learning Representations*.
- Meng, Y.; Bing, Z.; Yao, X.; Chen, K.; Huang, K.; Gao, Y.; Sun, F.; and Knoll, A. 2025. Preserving and Combining Knowledge in Robotic Lifelong Reinforcement Learning. *Nature Machine Intelligence*, 1–14.
- Mittal, S.; Bengio, Y.; and Lajoie, G. 2022. Is a Modular Architecture Enough? In Oh, A. H.; Agarwal, A.; Belgrave, D.; and Cho, K., eds., *Advances in Neural Information Processing Systems*.
- Mysore, S.; Cheng, G.; Zhao, Y.; Saenko, K.; and Wu, M. 2022. Multi-Critic Actor Learning: Teaching RL Policies to Act with Style. In *International Conference on Learning Representations*.
- Nachum, O.; Gu, S. S.; Lee, H.; and Levine, S. 2018. Data-Efficient Hierarchical Reinforcement Learning. In Bengio, S.; Wallach, H.; Larochelle, H.; Grauman, K.; Cesa-Bianchi, N.; and Garnett, R., eds., *Advances in Neural Information Processing Systems*, volume 31. Curran Associates, Inc.
- Nath, S.; Peridis, C.; Ben-Iwhiwhu, E.; Liu, X.; Dora, S.; Liu, C.; Kolouri, S.; and Soltoggio, A. 2023. Sharing Lifelong Reinforcement Learning Knowledge via Modulating Masks. In *Second Conference on Lifelong Learning Agents (CoLLAs) 2023*.
- Ostapenko, O.; Rodríguez, P.; Caccia, M.; and Charlin, L. 2021. Continual Learning via Local Module Composition. In *Proceedings of the 35th International Conference on Neural Information Processing Systems, NIPS '21*. Red Hook, NY, USA: Curran Associates Inc. ISBN 9781713845393.
- Parisi, G. I.; Kemker, R.; Part, J. L.; Kanan, C.; and Wermter, S. 2019. Continual Lifelong Learning with Neural Networks: A Review. *Neural Networks*, 113: 54–71.
- Rakelly, K.; Zhou, A.; Finn, C.; Levine, S.; and Quillen, D. 2019. Efficient Off-Policy Meta-Reinforcement Learning via Probabilistic Context Variables. In Chaudhuri, K.; and Salakhutdinov, R., eds., *Proceedings of the 36th International Conference on Machine Learning*, volume 97 of *Proceedings of Machine Learning Research*, 5331–5340. PMLR.
- Ramanujan, V.; Wortsman, M.; Kembhavi, A.; Farhadi, A.; and Rastegari, M. 2020. What’s Hidden in a Randomly Weighted Neural Network? In *Proceedings of the IEEE/CVF Conference on Computer Vision and Pattern Recognition*, 11893–11902.
- Ramé, A.; Couairon, G.; Shukor, M.; Dancette, C.; Gaya, J.-B.; Soulier, L.; and Cord, M. 2023. Rewarded Soups: Towards Pareto-optimal Alignment by Interpolating Weights Fine-tuned on Diverse Rewards. arXiv:2306.04488.
- Raposo, D.; Ritter, S.; Richards, B.; Lillicrap, T.; Humphreys, P. C.; and Santoro, A. 2024. Mixture-of-Depths: Dynamically Allocating Compute in Transformer-Based Language Models. arXiv:2404.02258.
- Rusu, A. A.; Rabinowitz, N. C.; Desjardins, G.; Soyer, H.; Kirkpatrick, J.; Kavukcuoglu, K.; Pascanu, R.; and Hassel, R. 2016. Progressive Neural Networks. *arXiv preprint arXiv:1606.04671*.
- Samvelyan, M.; Kirk, R.; Kurin, V.; Parker-Holder, J.; Jiang, M.; Hambro, E.; Petroni, F.; Kuttler, H.; Grefenstette, E.; and Rocktäschel, T. 2021. MiniHack the Planet: A Sandbox for Open-Ended Reinforcement Learning Research. In *Thirty-fifth Conference on Neural Information Processing Systems Datasets and Benchmarks Track (Round 1)*.
- Sartoretti, G.; Wu, Y.; Paivine, W.; Kumar, T. S.; Koenig, S.; and Choset, H. 2019. Distributed reinforcement learning for multi-robot decentralized collective construction. In *Distributed Autonomous Robotic Systems: The 14th International Symposium*, 35–49. Springer.
- Schulman, J.; Wolski, F.; Dhariwal, P.; Radford, A.; and Klimov, O. 2017. Proximal Policy Optimization Algorithms. *arXiv preprint arXiv:1707.06347*.
- Serra, J.; Suris, D.; Miron, M.; and Karatzoglou, A. 2018. Overcoming Catastrophic Forgetting with Hard Attention to the Task. In *International Conference on Machine Learning*, 4548–4557. PMLR.
- Shazeer, N.; Mirhoseini, A.; Maziarz, K.; Davis, A.; Le, Q.; Hinton, G.; and Dean, J. 2017. Outrageously Large Neural Networks: The Sparsely-Gated Mixture-of-Experts Layer. arXiv:1701.06538.
- Soltoggio, A.; Ben-Iwhiwhu, E.; Braverman, V.; Eaton, E.; Epstein, B.; Ge, Y.; Halperin, L.; How, J.; Itti, L.; Jacobs, M. A.; Kantharaju, P.; Le, L.; Lee, S.; Liu, X.; Monteiro, S. T.; Musliner, D.; Nath, S.; Panda, P.; Peridis, C.; Pirsivash, H.; Parekh, V.; Roy, K.; Shperberg, S.; Siegelmann, H. T.; Stone, P.; Vedder, K.; Wu, J.; Yang, L.; Zheng, G.; and Kolouri, S. 2024. A Collective AI via Lifelong Learning and Sharing at the Edge. *Nature Machine Intelligence*, 6(3): 251–264.
- Soltoggio, A.; Ben-Iwhiwhu, E.; Peridis, C.; Ladosz, P.; Dick, J.; Pilly, P. K.; and Kolouri, S. 2023. The configurable tree graph (CT-graph): measurable problems in partially observable and distal reward environments for lifelong reinforcement learning. arXiv:2302.10887.
- Standley, T.; Zamir, A.; Chen, D.; Guibas, L.; Malik, J.; and Savarese, S. 2020. Which Tasks Should Be Learned Together in Multi-task Learning? In III, H. D.; and Singh, A., eds., *Proceedings of the 37th International Conference on Machine Learning*, volume 119 of *Proceedings of Machine Learning Research*, 9120–9132. PMLR.
- Stooke, A.; Lee, K.; Abbeel, P.; and Laskin, M. 2021. Decoupling Representation Learning from Reinforcement Learning. In Meila, M.; and Zhang, T., eds., *Proceedings*

- of the 38th International Conference on Machine Learning, volume 139 of *Proceedings of Machine Learning Research*, 9870–9879. PMLR.
- Sukhbaatar, S.; Golovneva, O.; Sharma, V.; Xu, H.; Lin, X. V.; Rozière, B.; Kahn, J.; Li, D.; tau Yih, W.; Weston, J.; and Li, X. 2024. Branch-Train-MiX: Mixing Expert LLMs into a Mixture-of-Experts LLM. arXiv:2403.07816.
- Sun, L.; Zhang, H.; Xu, W.; and Tomizuka, M. 2022. PaCo: Parameter-Compositional Multi-task Reinforcement Learning. In Oh, A. H.; Agarwal, A.; Belgrave, D.; and Cho, K., eds., *Advances in Neural Information Processing Systems*.
- Sutton, R. S.; and Barto, A. G. 2018. *Reinforcement Learning: An Introduction*. Cambridge, MA, USA: A Bradford Book. ISBN 0262039249.
- Tan, Y.; Long, G.; Liu, L.; Zhou, T.; Lu, Q.; Jiang, J.; and Zhang, C. 2022. FedProto: Federated Prototype Learning across Heterogeneous Clients. In *AAAI Conference on Artificial Intelligence*.
- Tang, S.; Ye, R.; Xu, C.; Dong, X.; Chen, S.; and Wang, Y. 2024. Decentralized and Lifelong-Adaptive Multi-Agent Collaborative Learning. *CoRR*, abs/2403.06535.
- Tarale, P.; Rietman, E.; and Siegelmann, H. T. 2025. Distributed Multi-Agent Lifelong Learning. *Transactions on Machine Learning Research*.
- Wang, Y.; Zhang, Y.; and Coates, M. 2021. Graph Structure Aware Contrastive Knowledge Distillation for Incremental Learning in Recommender Systems. In *International Conference on Information and Knowledge Management, Proceedings*, 3518–3522. Association for Computing Machinery. ISBN 9781450384469.
- Wortsman, M.; Ilharco, G.; Gadre, S. Y.; Roelofs, R.; Gontijo-Lopes, R.; Morcos, A. S.; Namkoong, H.; Farhadi, A.; Carmon, Y.; Kornblith, S.; and Schmidt, L. 2022. Model Soups: Averaging Weights of Multiple Fine-Tuned Models Improves Accuracy Without Increasing Inference Time. In Chaudhuri, K.; Jegelka, S.; Song, L.; Szepesvari, C.; Niu, G.; and Sabato, S., eds., *Proceedings of the 39th International Conference on Machine Learning*, volume 162 of *Proceedings of Machine Learning Research*, 23965–23998. PMLR.
- Wortsman, M.; Ramanujan, V.; Liu, R.; Kembhavi, A.; Rastegari, M.; Yosinski, J.; and Farhadi, A. 2020. Supermasks in Superposition. *Advances in Neural Information Processing Systems*, 33: 15173–15184.
- Yadav, P.; Tam, D.; Choshen, L.; Raffel, C.; and Bansal, M. 2023. TIES-Merging: Resolving Interference When Merging Models. In *Proceedings of the 37th International Conference on Neural Information Processing Systems, NIPS '23*. Red Hook, NY, USA: Curran Associates Inc.
- Yarats, D.; Fergus, R.; Lazaric, A.; and Pinto, L. 2021. Reinforcement Learning with Prototypical Representations. arXiv:2102.11271.
- Yoon, J.; Jeong, W.; Lee, G.; Yang, E.; and Hwang, S. J. 2021. Federated Continual Learning with Weighted Inter-client Transfer. In Meila, M.; and Zhang, T., eds., *Proceedings of the 38th International Conference on Machine Learning*, volume 139 of *Proceedings of Machine Learning Research*, 12073–12086. PMLR.
- Yu, J.; Vincent, J. A.; and Schwager, M. 2022. DiNNO: Distributed Neural Network Optimization for Multi-Robot Collaborative Learning. *IEEE Robotics and Automation Letters*, 7(2): 1896–1903.
- Yu, T.; Kumar, S.; Gupta, A.; Levine, S.; Hausman, K.; and Finn, C. 2020. Gradient Surgery for Multi-Task Learning. In Larochelle, H.; Ranzato, M.; Hadsell, R.; Balcan, M.; and Lin, H., eds., *Advances in Neural Information Processing Systems*, volume 33, 5824–5836. Curran Associates, Inc.
- Zamir, A.; Sax, A.; Shen, W.; Guibas, L.; Malik, J.; and Savarese, S. 2018. Taskonomy: Disentangling Task Transfer Learning. arXiv:1804.08328.
- Zintgraf, L.; Schulze, S.; Lu, C.; Feng, L.; Igl, M.; Shiarlis, K.; Gal, Y.; Hofmann, K.; and Whiteson, S. 2021. VariBAD: Variational Bayes-Adaptive Deep RL via Meta-Learning. *J. Mach. Learn. Res.*, 22(1).

Symbol	Definition
Φ	Frozen backbone network
τ	Task τ
ϕ_τ	Randomly initialized learnable mask for task τ
ϕ_k	A mask acquired from a peer
π_τ	Policy for task τ
c	A communication event
P_c	A set of masks acquired from peers
$g(\cdot)$	Element-wise binarization function
ℓ	Layer ℓ of the network
γ^*	Optimal transport problem
v_τ	Wasserstein task embedding for task τ
μ_τ	Empirical distribution for task τ
μ_0	Fixed synthetic reference distribution
β	Learnable mixture weights for linear combination
θ	Cosine similarity threshold
\bar{r}	Normalized iteration reward scalar
N	Number of SAR samples for embedding computation
M	Number of reference points in the synthetic distribution
$\mathbb{I}_{\text{align}}$	Task similarity selection heuristic
\mathbb{I}_{perf}	Performance selection heuristic

Table 2: Table of important notations in the paper.

A Significance Testing

Deep reinforcement learning experiments exhibit substantial variability across random seeds and environment stochasticity (Henderson et al. 2018). To improve the robustness and interpretability of the results, we follow the recommendations of (Colas, Sigaud, and Oudeyer 2018) and report both confidence intervals and formal significance tests on the results.

For each benchmark, each algorithm is evaluated on multiple agents. For every agent, 5 independent algorithm seeds and 5 environment seeds. A difference test is computed using the Welch t-test and bootstrap confidence interval (BCI). Table 3 reports the results of this test for the results of each benchmark.

B Extended Related Work

This section provides additional information on the work related to MOSAIC and clarifies its unique contributions within the broader landscape.

Modular Representations and Masking. Modular policies promote parameter reuse by isolating task-specific sub-structures. Binary masks define sparse sub-regions of shared networks, reducing interference and enabling structured composition (Mallya, Davis, and Lazebnik 2018; Mallya and Lazebnik 2018; Ramanujan et al. 2020; Serra et al. 2018; Wortsman et al. 2020; Koster, Grothe, and Rettinger 2022). Some approaches compose masks to support task transfer (Ostapenko et al. 2021; Mendez, van Seijen, and Eaton 2022; Gummadi et al. 2022; Ben-Iwhiwhu et al. 2023). These methods typically require predefined task boundaries or centralized coordination. MOSAIC differs by enabling decentralized, performance-driven mask selection

without explicit task labels.

Mixture-of-Experts (MoE) architectures route inputs to sparse expert modules via learned gates (Shazeer et al. 2017; Fedus, Zoph, and Shazeer 2022), with variants adapted to multi-task and lifelong settings (Gururangan et al. 2020; Mendez and Eaton 2021). MOORE imposes orthogonality constraints across experts to promote representational diversity (Hendawy, Peters, and D’Eramo 2024). Related work in modular meta-learning emphasizes structural reuse through task-level module composition (Alet, Lozano-Perez, and Kaelbling 2018; Mittal, Bengio, and Lajoie 2022). These approaches require training routing mechanisms or meta-learning procedures. MOSAIC instead uses Wasserstein-based similarity to automatically select relevant modules without additional training overhead.

LoRA adds task-specific low-rank adapters to fixed models for efficient specialization (Hu et al. 2022). Neural Module Networks support compositional inference via dynamically assembled submodules (Andreas et al. 2016; Araki et al. 2021). MultiCriticAL isolates value functions per task to mitigate interference in actor-critic training (Mysore et al. 2022). Recent robotic lifelong learning systems adopt modular structures with Bayesian non-parametric inference to preserve and combine task-specific knowledge (Meng et al. 2025). Modular compositionality on policies enables agents to dynamically combine pre-trained skills to solve new tasks in a scalable and interpretable manner (Li et al. 2024). MOSAIC extends these ideas by combining binary mask modularity with performance-based selection and similarity-driven policy integration in a fully decentralized manner.

Task Similarity and Inference. Task inference enables modular adaptation without task labels. Latent and Bayesian models estimate embeddings from trajectories (Zintgraf et al. 2021; Achille et al. 2019). Non-parametric and prototype-based methods define task similarity via behavioral statistics (Yarats et al. 2021; Chu, Cai, and Wang 2024; Liu et al. 2025; Kolouri et al. 2021; Dick et al. 2024). Taskonomy (Zamir et al. 2018) and Task2Vec (Achille et al. 2019) provide task embeddings for transfer learning. Recent work explores which tasks benefit from joint learning (Standley et al. 2020). These methods typically require centralized computation or predefined task structures. MOSAIC computes Wasserstein-based similarity directly from agent trajectories in a decentralized fashion, enabling online task relationship discovery.

Wasserstein barycenter methods enable structure-aware ensembling by incorporating semantic side information through optimal transport distances (Dognin et al. 2019). Learning embeddings into entropic Wasserstein spaces offers a flexible alternative to Euclidean embeddings for capturing rich relational structures (Frogner, Mirzazadeh, and Solomon 2019). MOSAIC leverages these optimal transport principles specifically for RL trajectory comparison and module selection.

Contrastive objectives such as CURL (Laskin, Srinivas, and Abbeel 2020) and ATC (Stooke et al. 2021) improve representation learning, though they typically require encoder training and large batch sizes. Structure-aware distillation

CT-graph ISL				
Method	Final Perf (mean \pm 95% CI)	Δ (MOSAIC – Method)	Welch p (vs MOSAIC)	95% BCI of Δ
MOSAIC	0.91 [0.87, 0.95]	-	-	-
MOSAIC-NoComm	0.34 [0.26, 0.42]	0.58	1.74e-28	[0.49, 0.66]
MiniGrid Crossing				
Method	Final Perf (mean \pm 95% CI)	Δ (MOSAIC – Method)	Welch p (vs MOSAIC)	95% BCI of Δ
MOSAIC	0.83 [0.75, 0.90]	-	-	-
MOSAIC-NoComm	0.77 [0.68, 0.86]	0.06	3.26e-01	[-0.06, 0.18]
MOORE	0.63 [0.52, 0.74]	0.20	3.98e-03	[0.07, 0.32]
PCGrad+MoE	0.30 [0.20, 0.41]	0.53	6.37e-13	[0.39, 0.65]
MDQN	0.00 [0.00, 0.00]	0.83	3.82e-32	[0.75, 0.90]
MTPPO	0.21 [0.12, 0.31]	0.61	4.40e-18	[0.49, 0.73]
MiniHack MultiRoom				
Method	Final Perf (mean \pm 95% CI)	Δ (MOSAIC – Method)	Welch p (vs MOSAIC)	95% BCI of Δ
MOSAIC	0.64 [0.54, 0.74]	-	-	-
MOSAIC-NoComm	0.27 [0.15, 0.38]	0.37	2.06e-06	[0.22, 0.51]

Table 3: Total evaluation performance and significance testing CT-graph, MiniGrid and MiniHack benchmarks. Δ denotes MOSAIC – Method. Rows highlighted in green indicate methods for which MOSAIC is significantly better (Welch’s t -test $p < 0.05$ and 95% bootstrap CI of Δ excludes 0).

has also been explored in incremental graph-based settings (Wang, Zhang, and Coates 2021), offering another avenue for modular task inference. MOSAIC avoids the need for contrastive training by directly computing trajectory similarities for module selection.

Gradient-based meta-RL methods such as MAML (Finn, Abbeel, and Levine 2017) optimize for rapid task adaptation through fine-tuning, while variational approaches like VariBAD (Zintgraf et al. 2021) condition policy learning on inferred latent variables. In contrast, non-parametric methods that reuse task-conditional modules based on similarity measures offer an alternative path to fast generalization without the need for gradient-based adaptation. MOSAIC follows this non-parametric approach.

Model Merging and Upcycling. Emerging techniques enable the combination and repurposing of existing models through weight-space merging or routing. Wortsman et al. (2022) and Ramé et al. (2023) propose interpolating parameters from multiple fine-tuned models to improve generalization. TIES-Merging (Yadav et al. 2023) resolves interference between merged models. Komatsuzaki et al. (2023) and Sukhbaatar et al. (2024) demonstrate sparse upcycling: extracting sparse modular experts from dense checkpoints. These strategies provide alternatives to training from scratch and are critical for decentralized reuse. MOSAIC extends these ideas to multi-agent RL by combining similarity-driven linear policy combinations with binary mask modularity.

Adaptive and Elastic Architectures. Recent work explores modular and resource-aware architectures. MatFormer (Devvrit et al. 2024) and Mixture-of-Depths (Rapoza et al. 2024) dynamically allocate compute and ad-

just routing depths in transformer models. These approaches support efficient inference and specialization while preserving modular structure, principles aligned with our use of task-conditional module composition. MOSAIC applies similar principles to multi-agent systems through selective module reuse based on performance signals.

Hierarchical and Curriculum Learning. Hierarchical RL tackles long-horizon credit assignment and sparse reward signals. HAC (Levy et al. 2019) introduces layered actor-critic policies operating at different temporal resolutions. CAMRL (Huang et al. 2023) proposes curriculum-driven asymmetric MTRL between teacher and student agents. Our method complements these paradigms by achieving curriculum-like generalization via unsupervised trajectory similarity and decentralized reuse without explicit hierarchical structures.

Selective Transfer Learning. Selective transfer methods determine what and where to transfer knowledge. Chu, De La Torre, and Cohn (2013) introduces selective transfer machines for personalized learning. Jang et al. (2019) learns what and where to transfer in deep networks. SpotTune (Guo et al. 2018) enables adaptive fine-tuning through selective transfer. These methods typically operate in supervised settings with labeled tasks. MOSAIC extends selective transfer to decentralized multi-agent RL through Wasserstein-based similarity and performance signals.

C Extending MOSAIC to Lifelong Reinforcement Learning

MOSAIC can be naturally extended to a lifelong learning (LL) setting (De Lange et al. 2022; Kudithipudi et al. 2022),

in which each agent learns a sequence of tasks while minimizing catastrophic forgetting and promoting forward transfer. LL MOSAIC agents can exploit their knowledge integration capabilities to accumulate knowledge that may derive from other agents, or from their own learning on previously encountered tasks. MOSAIC employs knowledge composition approaches that were developed in the field of lifelong reinforcement learning (Ben-Iwhiwhu et al. 2023).

In the experimental settings for MOSAIC, however, we employed a one task per agent approach to maintain the focus on knowledge sharing and composition. This setting can be extended to a more general case in which one agent is not limited to learning one task. Therefore, MOSAIC can be easily adapted to a fully-fledged lifelong learning scenario by modifying the linear combination and β parameter adjustment.

Let agent i currently be learning task $\tau_k + 1$. Its mask is composed from three sources: the current task mask ϕ_{τ_k+1} , prior task masks $\{\phi_{\tau_k}\}_{k=1}^K$, and peer masks $\{\phi_j\}_{j=1}^n$, acquired from other agents. The composed mask for task τ_{k+1} for the forward pass is thus given by,

$$\phi_{\tau_{k+1}}^c = \beta_{\tau_{k+1}} \phi_{\tau_{k+1}} + \sum_{k=1}^k \beta_{\tau_k} \phi_{\tau_k} + \sum_{j=1}^n \beta_j \phi_j, \quad (10)$$

where each β is a scalar weight normalized via softmax. In this case, the initialization problem includes setting the weighting for previous task masks, the current task mask, and the newly acquired masks from other agents. One simple approach could simply be to extend Eq. (8) to

$$\beta_{\tau_{k+1}} = \frac{1}{3} + \frac{2}{3}r, \quad \beta_{\tau_k} = \frac{(1-r)}{3k}, \quad \beta_j = \frac{(1-r)}{3n}. \quad (11)$$

The addition of lifelong learning presents an additional challenge. Boundaries in the sequence of tasks learned by an agent need to be identified, so that a new mask can be learned for each new task. One solution to this could be to use the cosine similarity computed from the Wasserstein embeddings to monitor the incoming data stream and decide when a new task starts using statistical methods (Dick et al. 2020, 2024).

D Additional Ablation Studies

Comparison of Sharing Frequencies. An ablation study was conducted to assess the effects of communication frequency on MOSAIC’s performance in the image sequence learning benchmark. Specifically, comparing frequencies of 1, 5, 10 (default), 25, and 40 iterations, where the frequency indicates how often agents search, retrieve and compose peer masks. As shown in Figure 7, excessive communication (frequency of 1) results in performance degradation. In this setting, newly acquired masks continually override the agent’s own beta parameter adjustments, preventing meaningful adaptation and fine-tuning. Frequencies of 5 and 10 yield comparable early performance, with a frequency of 10 achieving higher final return. Conversely, with infrequent communication (25 or 40 iterations) agents have fewer opportunities for useful knowledge transfer, leading to weaker

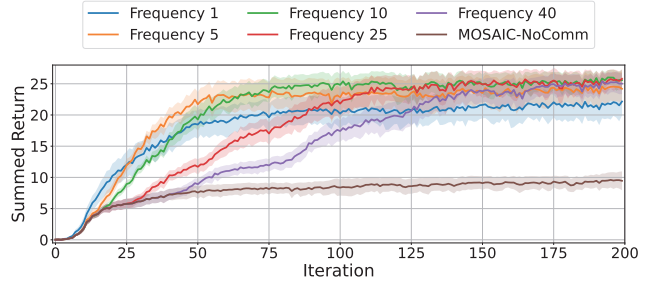


Figure 7: Comparison of MOSAIC with varying communication frequencies highlights the effect on performance in the image sequence learning problem. Striking the right balance in communication frequency is critical: infrequent communication can lead to missed performance gains, while communicating at every iteration may not allow sufficient time for effective local adaptation.

overall performance gains. These results highlight the importance of balancing between querying for peer knowledge often enough for a benefit to occur, and allowing agents to then tailor peer masks towards their own tasks.

Comparing Effects of Number of Samples and Reference Size on Embedding Similarity. We conducted a grid search on the number of samples per embedding N (Eq. (2)) and the size of the reference distribution M (Eq. (3)) to determine their effects on similarity computations and performance on the image sequence learning benchmark. Results shown in Figure 8 indicate no statistically significant changes from using different parameters of N and M , on the resulting performance.

However, Figures 9 and 10 indicate that using smaller values of N and M leads to increased knowledge reuse across task distributions. In more challenging settings, this may lead to catastrophic interference where misleading policies result in performance degradation. The effects of this are reduced in MOSAIC through the finetuning process in the linear combination of masks.

Table 4 reports the proportion of sharing within vs. cross-task distribution, for average cosine similarity and average beta parameter values. Within-cluster cosine similarity remains high across all configurations (0.84–0.88), indicating robust internal coherence among task groups. The cosine similarity between task distributions is more variable (0.38–0.43), with higher values observed at lower M , suggesting decreased separability between groups when mask capacity is restricted. Beta parameters exhibit a strong asymmetry: cross-distribution reuse is negligible (~ 0.000 – 0.003), while reuse within each cluster remains stable (~ 0.036 – 0.041). These trends confirm that agents primarily leverage intra-cluster task knowledge and that both sampling and masking hyperparameters influence the clarity and utility of the learned compositional structure.

E Additional Experiment Analysis

Figure 11 illustrates an example of the sequence-learning problem based on (Soltoggio et al. 2023). The agent must

Metric	N32 M50	N64 M50	N128 M10	N128 M20	N128 M30	N128 M50	N128 M70	N128 M100
Cross-Similarity	0.3887	0.3895	0.4288	0.4135	0.3993	0.4047	0.4054	0.3956
Within-Similarity	0.8779	0.8677	0.8425	0.8482	0.8559	0.8529	0.8576	0.8571
Cross-Beta	0.0021	0.0006	0.0029	0.0019	0.0013	0.0006	0.0006	0.0000
Within-Beta	0.0384	0.0368	0.0395	0.0377	0.0374	0.0386	0.0397	0.0411

Table 4: The average cross-cluster and within-cluster cosine similarity and beta parameter values across various N, M configurations. Average cosine similarity within clusters decreases as N and M increase. The average beta parameter values also increase as N and M increase, suggesting increased transfer between tasks driven by more accurate cosine similarity.

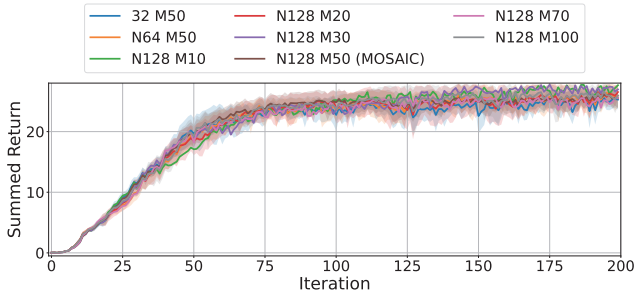


Figure 8: Comparison of MOSAIC with varying communication frequencies highlights the effect on performance in the image sequence learning problem. Striking the right balance in communication frequency is critical: infrequent communication can lead to missed performance gains, while communicating at every iteration may not allow sufficient time for effective local adaptation.

navigate a series of nodes labeled as H (home), W (wait state), D (decision state), and R (reward state). For the experiments in this paper, the wait state probability is set to zero, resulting in reduced complexity.

Figure 12 shows examples of the MiniGrid curriculum used in our MiniGrid Crossing experiments. Agents are expected to learn useful behaviors/trajectories to navigate around obstacles in the form of walls or lava, and reach the goal state (green). This setup tests to see if agents can identify similarities in the structure of the tasks, irrespective of the changing observations (wall, lava), and transfer useful policies from SimpleCrossing to LavaCrossing variations, as well as on other SimpleCrossing/LavaCrossing variations.

Figure 13 shows an example of a MiniHack MultiRoom task. The start and goal states are represented by squares with up and down arrows, respectively. The agent is expected to navigate through each room, learning to navigate towards and open doors along the way until it reaches the goal state in the final room.

Figures 14, 15, and 16 show the individual task performance curves for the image sequence learning setting, MiniHack MultiRoom, and MiniGrid Crossing, respectively.

E.1 Further Analysis of Similarity and Converged Beta Parameters

The image sequence learning benchmark consists of four distinct image datasets, resulting in four independent state

spaces. Four unique trajectories are chosen, one for each image dataset. Seven hierarchically related tasks are selected from each trajectory-dataset combination resulting in a total of 28 tasks with four clusters denoted by (0 to 6), (7 to 13), (14 to 20), (21 to 27). Figure 17 shows the annotated results of the heatmaps presented in Figure 4(D) and (E) for each of these clusters, identified by the WPGMA (Figure 4(C)).

Figure 18(top) shows the distributions of pairwise cosine similarities between groups of tasks. Pairs are grouped as either *Within Distributions*, where both tasks share the same image dataset and trajectory (e.g., Dataset 1-Dataset 1), or *Across Distributions*, where tasks come from different datasets and trajectories (e.g., Dataset 1-Dataset 3). Tasks within the same distribution show significantly higher similarity, indicating that MOSAIC embeddings reflect shared perceptual features and curriculum alignment. The MiniHack benchmark extends the MiniGrid MultiRoom curriculum. It consists of tasks ranging from two to eight rooms in size, with task IDs 0–6 corresponding to room size 4×4 and tasks 7–13 to size 6×6 . Canonical pairs are defined by room count; for example, task 0 and task 7 are both 2-room versions of different sizes. Cosine similarity analysis reveals clear grouping by room size, with tasks within the same spatial resolution exhibiting stronger similarity than canonical pairs across sizes, indicating that visual and navigational complexity induced by room dimensions plays a more significant role in shaping the embedding space than shared structural depth alone.

The matrix $\hat{\beta}$ shows that knowledge reuse in MiniHack occurs predominantly within the same room size group. Smaller tasks, such as the 2-room and 3-room configurations, are reused more frequently and earlier in training, consistent with their faster convergence. As in MiniGrid, structural pairing alone does not guarantee high reuse. Figure 18(middle) shows that canonical pairs (e.g., 0–7, 1–8) have only moderate similarity, while many within-group pairs yield stronger transfer potential. The dominance of reuse within room size groups may also be explained in part by the timing of performance gains. Tasks with smaller rooms converge earlier and thus become eligible for reuse earlier, which reinforces their influence even when structurally similar tasks emerge later in training. In the MiniGrid benchmark, tasks are divided into two families: SimpleCrossing (SC; tasks 0–6) and LavaCrossing (LC; tasks 7–13). Each SC task has a corresponding LC task with a matched structural layout but different obstacles (walls versus lava), forming seven pairs of canonical tasks (e.g. 0-

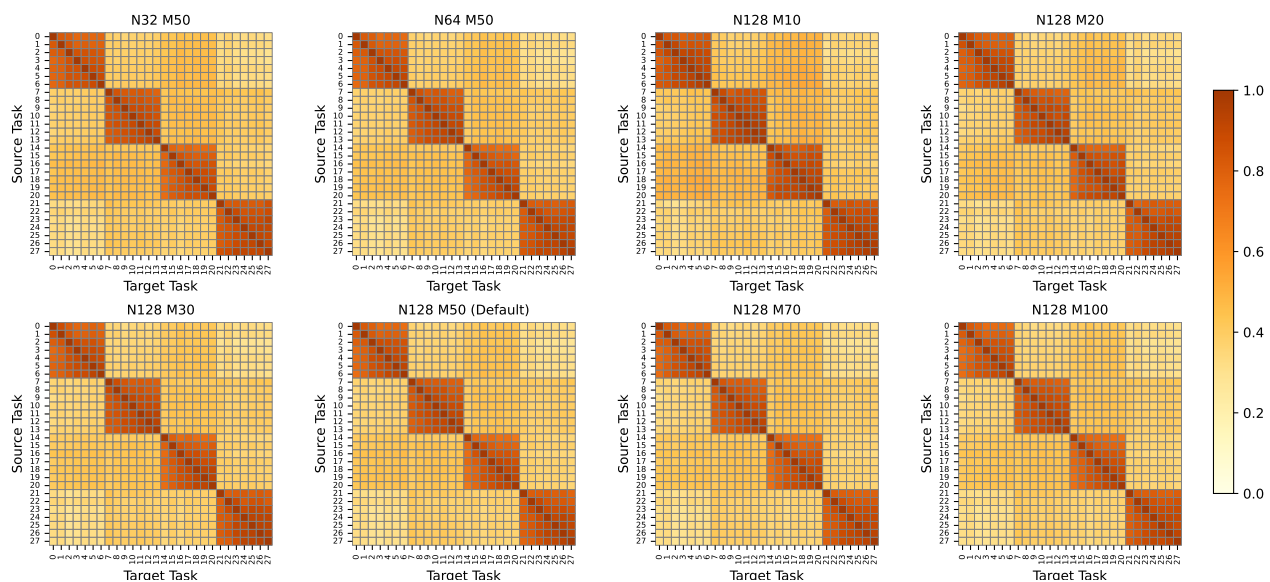


Figure 9: Cosine similarity heatmaps for configurations of N and M . Cross-cluster cosine similarity increases with smaller values of N and M , leading to instances of cross-cluster sharing. Higher values increase the accuracy of embedding cosine similarity.

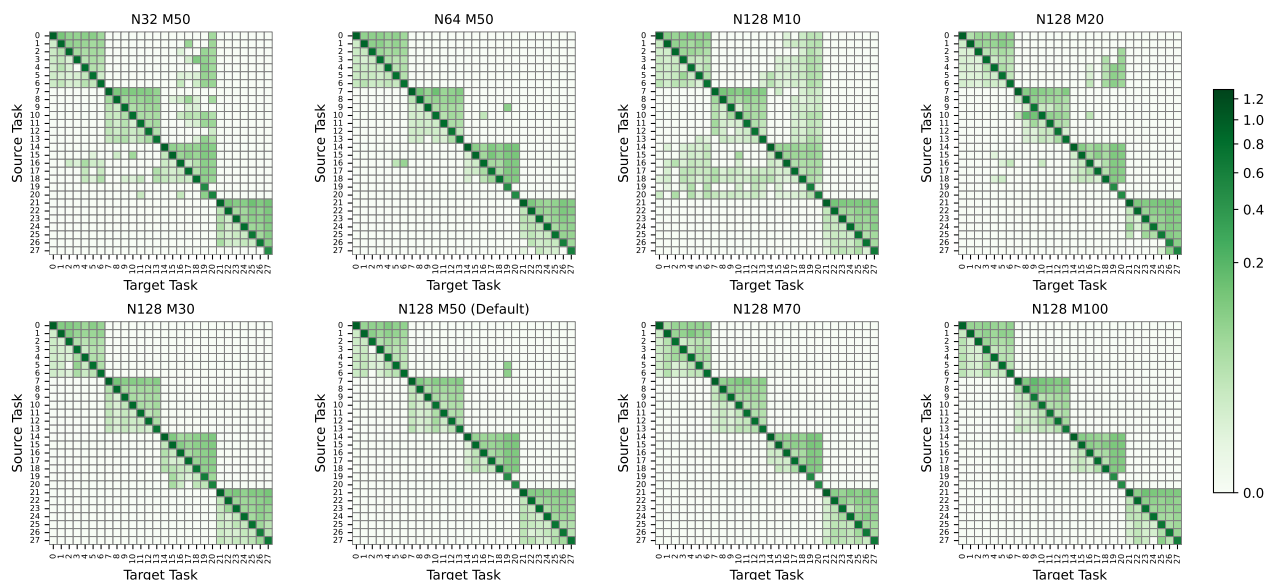


Figure 10: Beta parameters heatmaps for configurations of N and M . Less accurate cosine similarity estimates result in the transfer of masks. This then leads to the reuse of these masks in the linear combination.

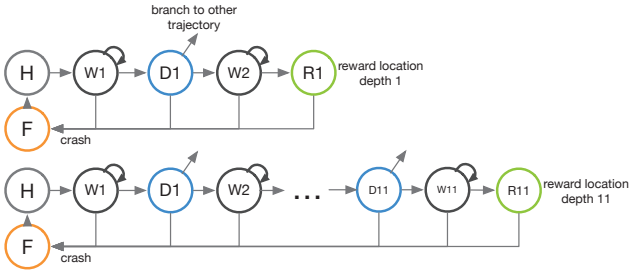


Figure 11: Illustration of the image sequence learning problem. Each graph is comprised of various states, represented by procedurally generated images. The agent must learn to navigate these image states and acquire a sparse reward. (Top) shows an example of a depth-1 graph. Bottom shows a depth 11 graph along the same trajectory.

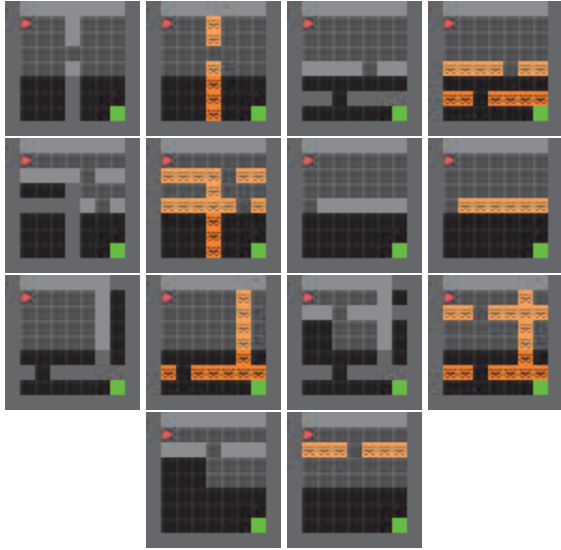


Figure 12: Illustrations of the MiniGrid SimpleCrossing and LavaCrossing curriculum used in our experiments. Each SimpleCrossing variation is accompanied by a LavaCrossing counterpart. This approach tests whether MOSAIC agents can transfer knowledge across different observation spaces while maintaining agent specialization.

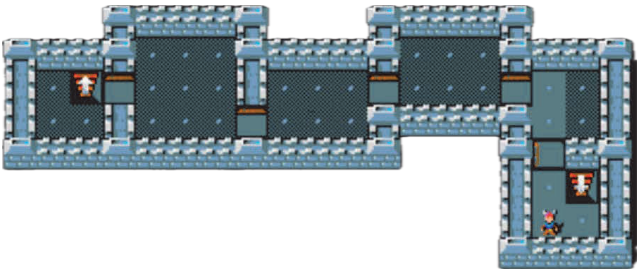


Figure 13: Example illustration of the MiniHack MultiRoom benchmark. Each environment consists of multiple rooms of varying sizes, connected by closed (but unlocked) doors. Tiles with upwards arrows indicate starting locations, and tiles with downwards arrows indicate goal locations.

7, 1-8) that are structurally similar. Surprisingly, the pairwise cosine similarity heatmap reveals that these canonical pairs do not generally have the highest similarity. Instead, many within-family pairs show stronger similarity, particularly among SC tasks. Many non-structurally matched pairs also exhibit unexpectedly high similarity. These results suggest that actual knowledge reuse in MOSAIC is non-trivial. Rather MOSAIC agents likely reuse policies with relevant sub-trajectories that encoded in the Wasserstein task embeddings.

Figure 18(bottom) categorizes task pairs into three groups: *Structurally Matched Pairs (SC-LC)*, consisting of canonical SimpleCrossing-LavaCrossing pairs with identical map layouts; *Same Task Type (SC-SC or LC-LC)*, where both tasks share common states but differ in layout; and *Non-Structurally Matched Pairs*, which includes all remaining SC-LC task pairs not matched by structure. Structurally matched pairs do not show higher similarity than within-type pairs, suggesting that embedding similarity is more influenced by task dynamics than map layout.

The corresponding $\hat{\beta}$ matrix (Figure 20) indicates that knowledge reuse in MiniGrid is selective and is not determined solely by the canonical structure. Reuse tends to favor structurally simple or early-learned tasks rather than those with the highest embedding similarity. Figure 18(bottom) confirms this pattern: canonical pairs show lower average similarity than both within-group and non-structurally-matched pairs, suggesting that MOSAIC’s embedding space captures aspects of task dynamics that go beyond explicit structural symmetry. Reuse decisions are shaped not only by similarity but also by policy quality and learning progress. This pattern may also reflect the temporal bias in reuse. Tasks such as SC0, which reach high performance early in training, become preferred sources of knowledge. Structurally matched tasks that appear later in training are often underutilized, due to the performance-based selection mechanism (criterion 2) that filters knowledge transfer based on relative performance.

F Implementation Details

In this section we provide implementation details for the MOSAIC algorithm. MOSAIC computes embeddings from batches of state-action-reward (SAR) data collected under the current policy. These embeddings evolve over time as the policy improves. Knowledge reuse is governed by a linear combination of task-specific masks selected using similarity and performance heuristics. The linear combination is weighted by learned β parameters which are re-initialized at each communication event, and then fine-tuned again to reflect downstream utility to the current task.

Algorithm 4 provides pseudocode for how MOSAIC computes the forward pass using a linear combination of masks and the binarization step. Algorithm 1 provides an outline of the main algorithmic pipeline. The agent additionally, runs two parallel threads to run and maintain interaction communication module and model while maintaining asynchronous operation. This enables MOSAIC to learn and communicate concurrently. Pseudocode for these threads are

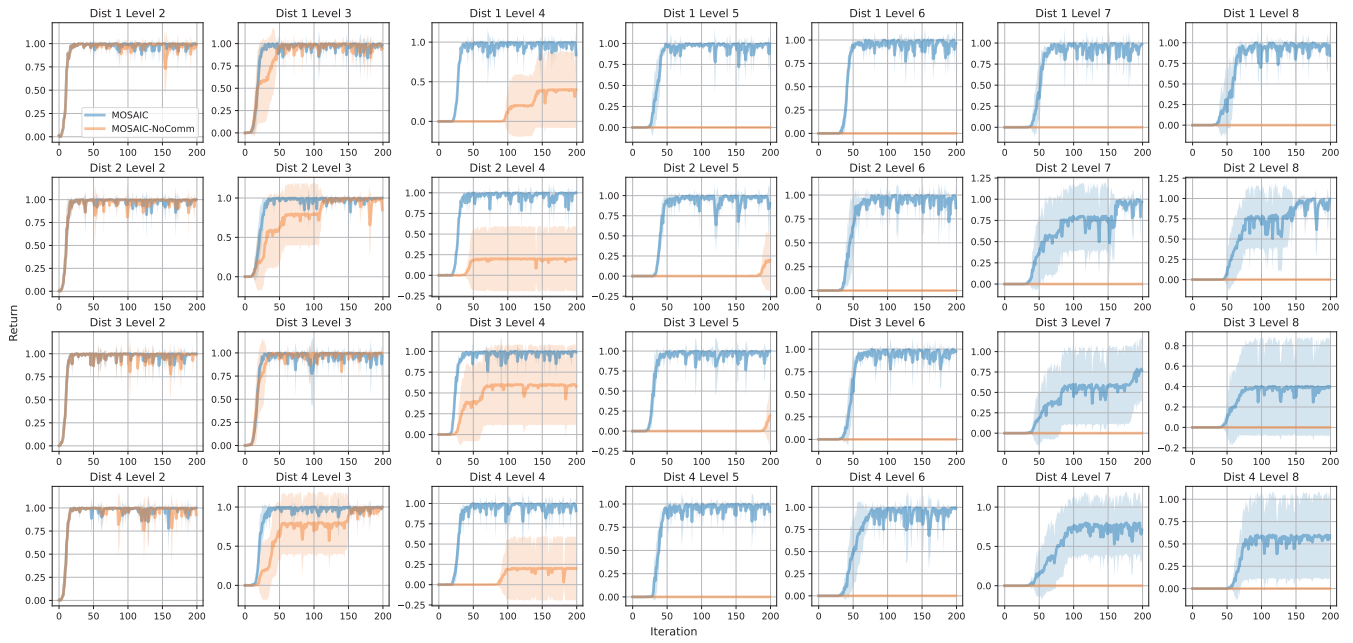


Figure 14: Individual task performance on the ISL benchmark.

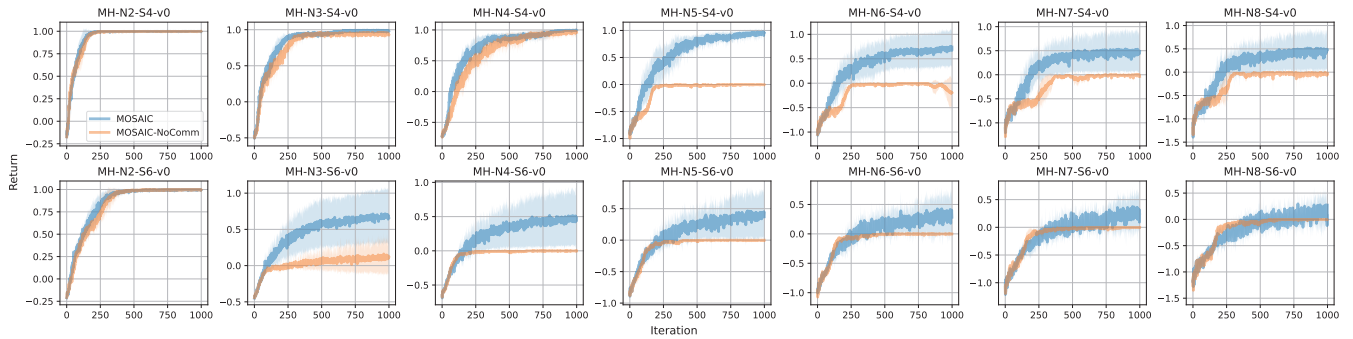


Figure 15: Individual task performance on the MiniHack benchmark.

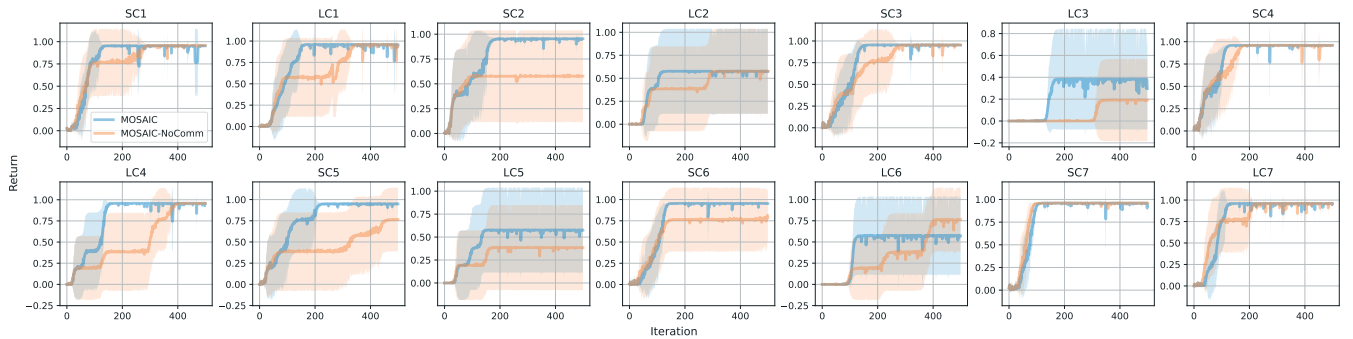


Figure 16: Individual task performance on the MiniGrid benchmark.

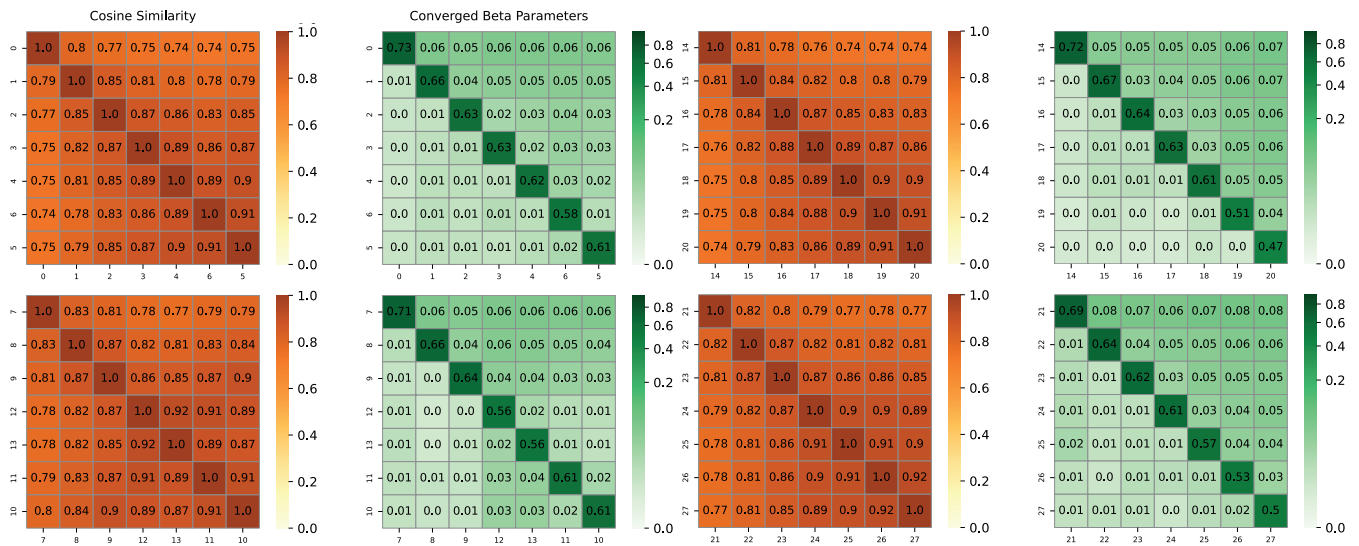


Figure 17: Individual heatmaps of each task distribution cluster from the image sequence learning results shown in Figure 4. Cosine similarity is highest between each task and the next task. Beta parameters indicate that cosine similarity has an inversely proportional relationship with cosine similarity, with foundational prior tasks having more weight. E.g., task 0 has the most weight for reuse in task 5.

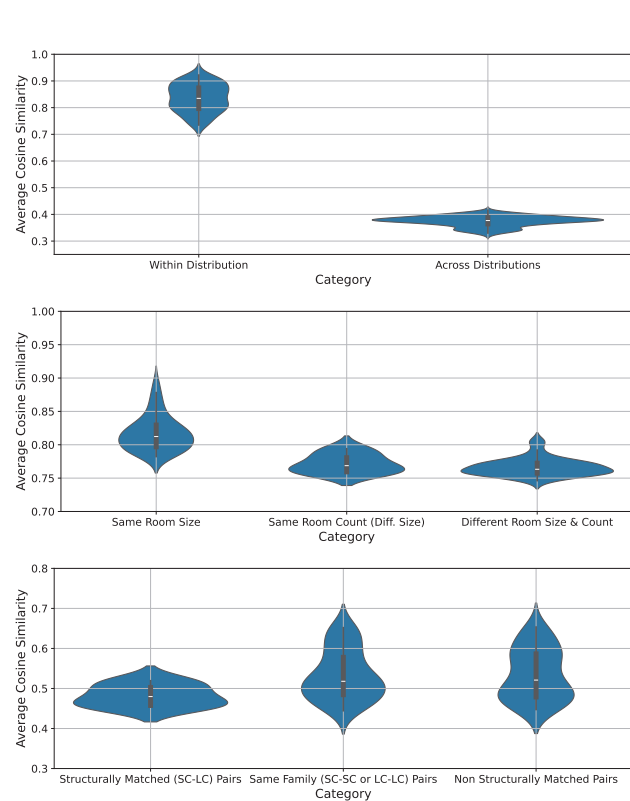


Figure 18: Violin plot showing the distribution of pairwise cosine similarities between task embeddings in the image sequence learning benchmark (top), MiniHack MultiRoom (middle), and MiniGrid Crossing (bottom).

provided in Algorithms 2 and 3. The server to accept incoming communications is started as a parallel process inside the communication module, described in Algorithm 5. Queries and masks are shared around the system via multiprocessing queues Q_{emb} and Q_{mask} . Algorithm 6 shows the computation of the Wasserstein task embeddings.

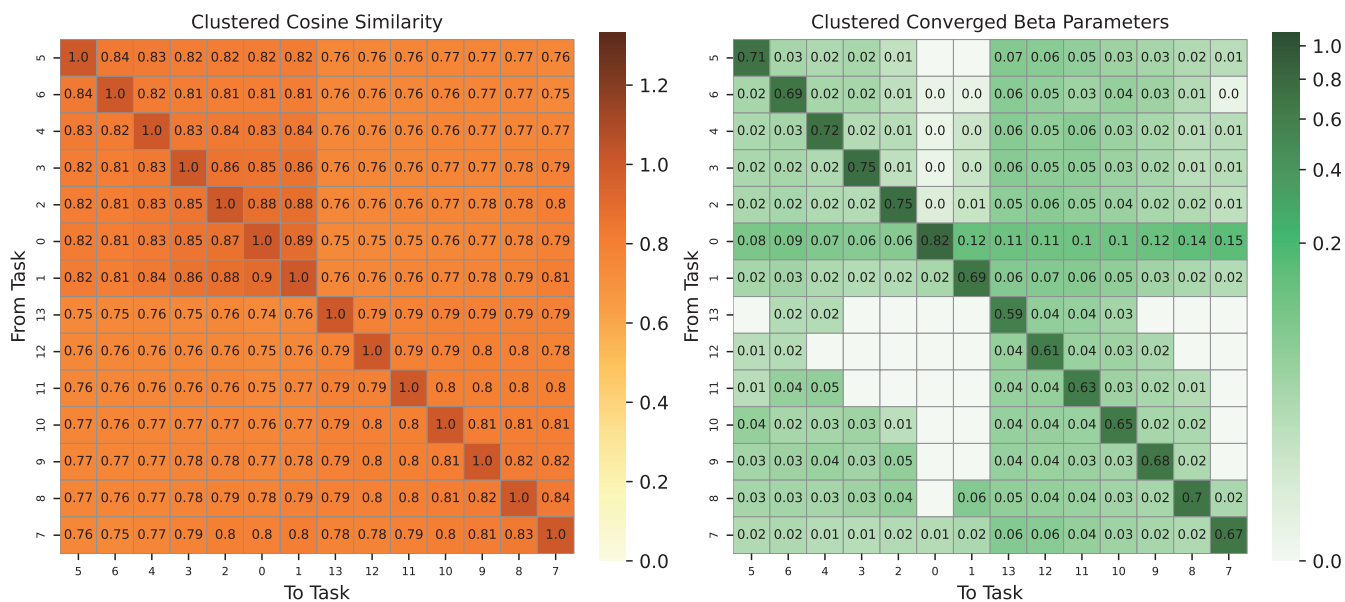


Figure 19: Pairwise (Left) cosine similarity and (Right) converged beta parameters results from the MiniHack experiment. Results are clustered using the WPGMA method.

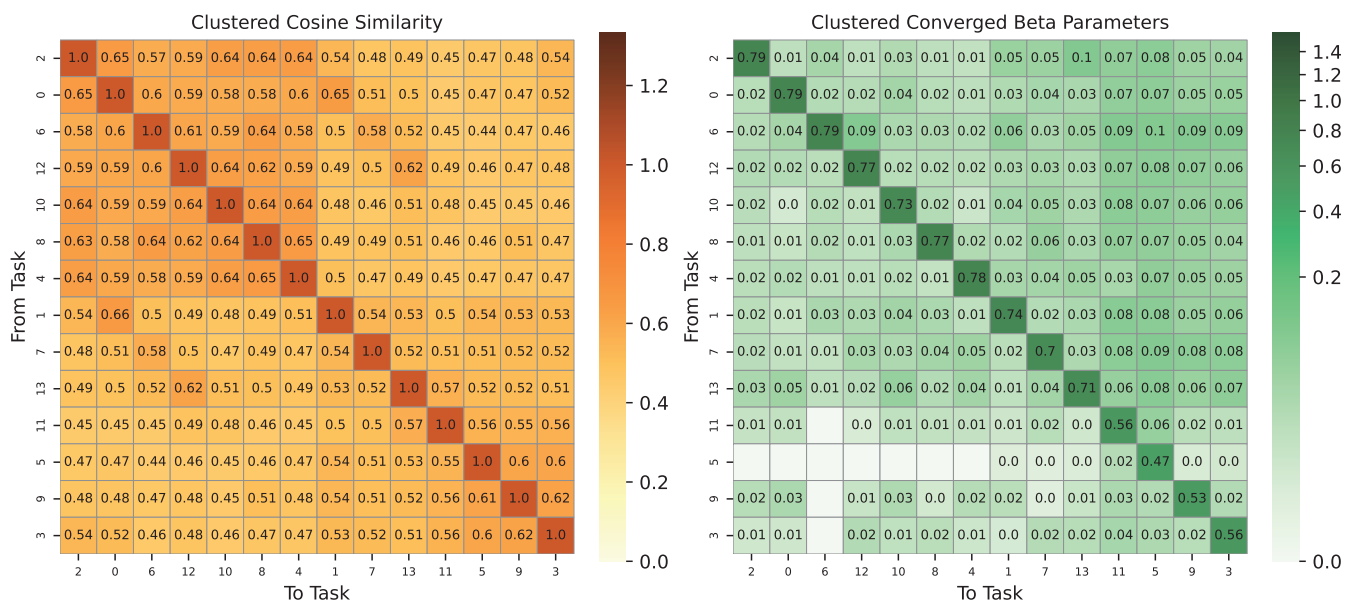


Figure 20: Pairwise (Left) cosine similarity and (Right) converged beta parameters results from the MiniGrid experiment. Results are clustered using the WPGMA method, revealing two distinct distributions. Task IDs 0-6 correspond to the SimpleCrossing. Tasks 7-13 correspond to the LavaCrossing. The results indicate that the cosine similarity of Wasserstein task embeddings is able to uncover meaningful relationships.

Algorithm 1: Agent Training Loop in MOSAIC

Require: Assigned task $\tau \in \mathcal{T}$, shared backbone Φ

Require: Communication event interval Δ_{comm} , embedding interval Δ_{embed}

Require: Replay buffer \mathcal{D}_τ , rollout length z , total steps Ω , cosine similarity threshold $\theta = 0.5$, $N \leftarrow 128$

```
1: Initialize mask  $\phi_\tau$ , embedding  $v_\tau \leftarrow \mathbf{0}$ , return estimate  $r \leftarrow 0$ , step counter  $t \leftarrow 0$ 
2: Initialize peer mask set  $P_0 = \emptyset$ , and linear combination parameters  $\beta \in \mathbb{R}^{1+|P_0|}$ 
3: Launch parallel threads:
4:   REPLACEPEERMASKS( $Q_{\text{mask}}$ ) ▷ Receives and applies mask updates Alg. 2
   COMMUNICATIONMODULE( $Q_{\text{emb}}, Q_{\text{mask}}$ ) ▷ Handles queries and peer responses Alg. 3
5: while  $t < \Omega$  do
6:   Roll out policy  $\pi_\tau = \pi_{\Phi \circ g(\phi_\tau^e)}$  for  $z$  steps ▷ Forward pass Alg. 4
7:   Store transitions in  $\mathcal{D}_\tau$ ; update iteration return estimate  $r$ 
8:   Update  $\phi_\tau$  using policy gradient on loss  $\mathcal{L}(\pi_\tau)$  ▷ Via Eq. 7
9:    $t \leftarrow t + z$ 
10:  if  $t \bmod \Delta_{\text{embed}} = 0$  and  $|\mathcal{D}_\tau| \geq N$  then
11:    Sample  $N$  samples from  $\mathcal{D}_\tau$  and compute task embedding  $v_\tau \leftarrow \psi(\mu_\tau)$  ▷ Alg. 6
12:  end if
13:  if  $t \bmod \Delta_{\text{comm}} = 0$  then
14:    Send TEQ for  $(v_\tau, r)$  to COMMUNICATIONMODULE via  $Q_{\text{emb}}$  and acquire set of peer masks  $P_{c+1} = \{\phi_1 \dots \phi_K\}$  in
    COMMUNICATIONMODULE
15:    Update model with  $P_{c+1}$  for forward pass via REPLACEPEERMASKS through  $Q_{\text{mask}}$ 
16:  end if
17:  if  $t = \Omega$  then
18:    Enter idle mode to keep COMMUNICATIONMODULE active
19:  end if
20: end while
```

Algorithm 2: Updating set of peer masks and resetting linear combination parameters

Require: latest iteration return r

```
1: procedure REPLACEPEERMASKS( $Q_{\text{mask}}$ )
2:   while running do
3:     Wait for set of new peer masks  $P_{c+1} = \{\phi_1^{\text{new}}, \dots, \phi_K^{\text{new}}\}$  from  $Q_{\text{mask}}$ 
4:     Update  $\phi_\tau \leftarrow \beta_\tau \phi_\tau + \sum_{k \in P_c} \beta_k \phi_k$  ▷ Consolidation step
5:     Cache consolidated mask for forward pass
6:     Update  $\beta_\tau \leftarrow 0.5 + 0.5r$ ,  $\beta_k \leftarrow \frac{0.5(1-r)}{|P_{c+1}|} \quad \forall k \in P_{c+1}$ 
7:      $P_c \leftarrow P_{c+1}$ 
8:   end while
9: end procedure
```

Algorithm 3: MOSAIC Communication Module

Require: Agent's IP/Port addr_i , Communication graph $\mathcal{G} = \{\mathcal{I}, \mathcal{E}\}$, where $\mathcal{E} = \{(i, j) \mid i, j \in \mathcal{I}, i \neq j\}$

```
1: procedure COMMUNICATIONMODULE( $Q_{\text{emb}}, Q_{\text{mask}}$ )
2:   Initialize parallel process COMMUNICATIONSERVER( $Q_{\text{MASK}}$ ) ▷ Begins server process Alg. 5
3:   while running do
4:     Wait for query  $(v_i, r_i, \text{addr}_i)$  from  $Q_{\text{emb}}$ 
5:     Send query to known peers
6:     Wait for set of peer QRs  $\{(v_j, r_j, \text{mask\_id}_j, \text{addr}_j)\}$  from COMMUNICATIONSERVER
7:     Select peers  $P \leftarrow \{j \mid \mathbb{I}_{\text{align}} \text{ and } \mathbb{I}_{\text{perf}}\}$ 
8:     Send mask request (MR) to selected peers  $P$ 
9:     Wait for peer masks from COMMUNICATIONSERVER and send to model via  $Q_{\text{mask}}$ 
10:  end while
11: end procedure
```

Algorithm 4: Forward pass using masks for network layer l

Require: Masks ϕ_τ , peer mask set $P = \{\phi_k\}_{k=1}^{|P|}$, parameters $\beta_\tau, \{\beta_k\}_{k=1}^{|P|}$, backbone Φ

```
1: procedure FORWARDPASS( $\mathbf{x}$ )
2:   if  $|P| = 0$  then ▷ no peer masks available
3:     Set  $\phi_\tau^{\text{lc}} \leftarrow \phi_\tau$ 
4:   else
5:      $\phi_\tau^{\text{lc}} \leftarrow g(\beta_\tau \phi_\tau + \sum_{k \in P} \beta_k \phi_k)$  ▷ Eq. 7
6:   end if
7:    $\pi_\tau \leftarrow \pi_{\Phi \odot \phi_\tau^{\text{lc}}}$  ▷ Modulate backbone with LC mask to get policy
8:    $y \leftarrow \pi_\tau \cdot \mathbf{x}$  ▷ Compute output from policy
9:   return  $y$ 
10: end procedure
```

Algorithm 5: Communication server

Require: World size W , Agent's IP/Port addr_i

```
1: procedure COMMUNICATIONSERVER( $Q_{\text{mask}}$ )
2:   Bind TCP socket to ( $\text{addr}_i$ )
3:   Listen for connections with backlog size  $W$ 
4:   while running do
5:     Accept incoming connection ( $\text{conn}, \text{remote\_addr}$ )
6:     Receive message from connection
7:     if message is an TEQ then
8:       if Server-side selection then
9:         Select mask(s) and respond with MTR to  $\text{remote\_addr}$ 
10:      else
11:        Respond to  $\text{remote\_addr}$  with embedding and performance (QR)
12:      end if
13:    else if message is an QR then
14:      Store QR ( $v_j, r_j, \text{mask\_id}, \text{addr}_j$ ) in set of query responses
15:    else if message is an MR then
16:      Fetch corresponding mask for mask id and respond to  $\text{remote\_addr}$  with MTR
17:    else if message is an MTR then
18:      Add mask to set of acquired peer masks
19:    end if
20:  end while
21: end procedure
```

Algorithm 6: Wasserstein Embedding Computation

```
1: procedure COMPUTEEMBEDDING( $\mathcal{D}$ )
2:   Compute embedding  $v_\tau^{\text{new}} \leftarrow \psi(\mathcal{D})$  ▷ via Eq. 5
3:    $v_\tau \leftarrow \frac{1}{2}(v_\tau + v_\tau^{\text{new}})$  ▷ Moving average update
4:   return  $v_\tau$ 
5: end procedure
```

System 1	
OS	Ubuntu 22.04.5 LTS
CPU	AMD EPYC 9634 (168 logical cores)
GPU(s)	2× NVIDIA A100 80GB PCIe
GPU Driver	535.216.03
CUDA Version	12.2
RAM	512 GB
System 2	
OS	Ubuntu 22.04.5 LTS
CPU	AMD EPYC 7713P (128 logical cores)
GPU(s)	2× NVIDIA A100 40GB PCIe
GPU Driver	535.216.03
CUDA Version	12.2
RAM	256 GB
System 3	
OS	Ubuntu 22.04.5 LTS
CPU	AMD Ryzen 9 5950X (32 logical cores)
GPU(s)	1× NVIDIA GeForce RTX 4090
GPU Driver	535.183.01
CUDA Version	12.2
RAM	128 GB

Table 5: Compute resources used to run the experiments presented in this paper for MOSAIC and baselines. We made use of the MiG configurations that are supported by the NVIDIA A100 GPUs to run each MOSAIC agent with its own instance. This configuration limits the effects of one agent on another from a hardware perspective.

Module	Hyperparameter	Value (ISL, MiniGrid, MiniHack)
PPO	Learning rate	0.00025
	Backbone seed	9157
	Number of workers	1
	Discount factor	0.99
	GAE Tau	0.99
	Entropy	0.01
	Rollout length	512 (ISL), 2048 (MiniGrid, MiniHack)
	Optimization iterations	8
	Mini-batches	64
	PPO ratio clip	0.1
	Gradient clip	5
Total training steps	102,400 (ISL), 1,024,000 (MiniGrid), 2,048,000 (MiniHack)	
Comm.	Query frequency (iterations)	10 (ISL, MiniHack), 25 (MiniGrid)
	Query wait (ms)	0.3
	Mask wait (ms)	0.3
Embedding	Reference size (M)	50
	Number of samples (N)	128
	Frequency (iterations)	1

Table 6: Hyperparameters used in the experiments presented in this paper. Values are provided for the reinforcement learning algorithm, the communication module and embedding module.

Package/Framework	Version
Python	3.9.13
PyTorch	2.4.0
TorchVision	0.19.0
TorchAudio	2.4.0
NumPy	1.24.3
SciPy	1.10.1
Pandas	2.2.2
Scikit-learn	1.5.1
Gym	0.26.0
Gym-Minigrid	1.2.2
Gym-CTGraph	0.1 (dev)
OpenCV-Python	4.10.0.84
Matplotlib	3.9.2
Seaborn	0.13.2
TensorBoardX	2.6.2.2
POT (Optimal Transport)	0.9.4
CUDA Toolkit	12.1.105
cuDNN	9.1.0

Table 7: Software packages and frameworks used for reproducibility.

Network	Architecture Details
Fully Connected	Feature extractor: Linear (input, 200) \rightarrow Linear (200, 200) \rightarrow Linear (200, 200) Critic: Linear (200, 1) Actor: Linear (200, action)
Convolutional	Feature extractor: Conv (input, 16, kernel 8, stride 4) \rightarrow Conv (16, 32, kernel 4, stride 2) \rightarrow Linear (8192, 256) Critic: Linear (256, 1) Actor: Linear (256, action)

Table 8: Network architectures used in experiments. Image sequence learning and MiniGrid benchmarks were run using the full connected network. MiniHack experiments were run using the convolutional network